NGU Report 2008.072

HeatBar Progress Report 2008
Basement characterization
Barents Sea and Svalbard

NGU
Norges geologiske undersøkelse
Geological Survey of Norway

Geological Survey of Norway
NO-7491 Trondheim, Norway
Tel.: 47 73 90 40 11
Telefax 47 73 92 16 20

REPORT

Report no.: 2008.072	ISSN	Grading: Open

Title:
HeatBar Report 2008, Basement Heat Generation and Heat Flow in the western Barents Sea - Importance for hydrocarbon systems

Authors:
Christophe Pascal, Cécile Barrère, Børre Davidsen, Jörg Ebbing, Harald Elvebakk, Laurent Gernigon, Odleiv Olesen, David Roberts, Anna Siedlecka, Jan Reidar Skilbrei, Trond Slagstad and Bjørn Wissing

Client:
StatoilHydro ASA

County:
Finnmark

Commune:

Map-sheet name (M=1:250.000)

Number of pages: 64 Price (NOK): 320,-
Map enclosures:

Fieldwork carried out:	Date of report:	Project no.:	Person responsible:
2006-2007	01.10.2008	3127.00	Kjetil Nordgulen

Summary:

The HeatBar project aims to determine the relative proportion of heat originating in the basement of the western Barents Sea and, as such, follows the methodologies and scientific approach developed in the course of the 2005-2008 Kontiki Project. We propose to shed new lights on the thermal state of the basins of the western Barents Sea by (1) determining the heat flow and the relative content in heat-producing elements of the basement onshore northern Norway, (2) building 3D structural models of the basement offshore based on extensive geophysical information and (3) building 3D thermal models of the basins offshore. The present report summarises the work accomplished in the framework of the HeatBar project since 2006. Dense gravity and magnetic datagrids constrained by available seismics have been used to determine the nature of the basement underlying offshore sedimentary basins and to build preliminary 2D structural models. Two drillholes have been logged for temperature in Båtsfordfjellet and Bjørnevatn in eastern Finnmark and, when available, core material has been used for measuring thermal conductivities. Uncorrected heat flow values at the two sites are 25 and 66 (preferred) mW/m^2 respectively. The onshore basement in Finnmark has been extensively sampled for geochemical analyses and new heat-production data will become available very soon. Preliminary results from the very first datings of offshore basement samples are also presented. The results obtained so far will be used in the forthcoming thermal modelling effort.

Keywords: Geofysikk (Geophysics)	Kontinentalsokkel (Continental shelf)	Tolkning (Interpretation)
Varmestrøm (Heat flow)	Magnetometri (Magnetometry)	Berggrunnsgeologi (Bedrock geology)
Petrofysikk (Petrophysics)	Gravimetri (Gravimetry)	Fagrapport (Scientific report)

CONTENTS

1 INTRODUCTION

Understanding heat flow variation in sedimentary basins is of vital importance for the success of petroleum exploration campaigns. While oil industry has invested much in understanding the thermal input related to lithospheric thinning, it appears that comparatively little has been done on the subject of heat flow from different basement types. In 2004, Statoil and NGU decided to establish the Kontiki Project (Continental Crust and Heat Generation In 3D) to improve the knowledge on the varying heat flow on the Norwegian continental shelf. Kontiki was terminated in 2007 and the HeatBar Project is a sister project aiming to apply a similar approach to the western Barents Sea area.

Approximately half of the heat flow in thermally-relaxed sedimentary basins (i.e. older than 60 Myr) originates in the crystalline basement while the other half comes from the mantle (e.g. Ritter *et al.* 2004). The heat production within the crystalline basement depends on the content of radioactive elements such as potassium, uranium and thorium. The content of these elements shows a wide variation within the mainland crystalline basement of Norway. Partly due to a lack of systematic data compilation, the knowledge of the basement rock composition below the Norwegian continental shelf is very poor or almost non-existing in large areas.

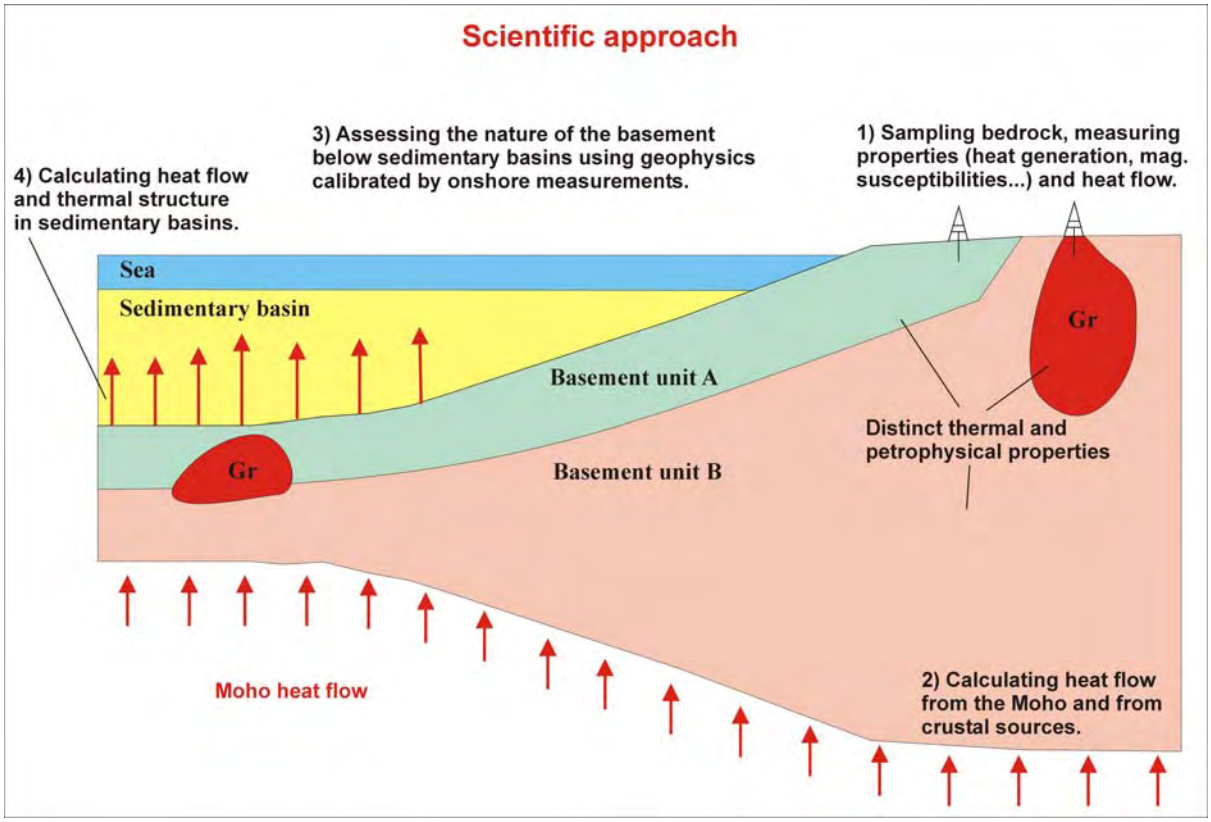

Figure 1.1. The Kontiki and HeatBar scientific approach.

Relatively acidic rocks of the Precambrian gneisses and granites generate more heat than intermediate-mafic rocks within the Caledonian nappes and high-grade metamorphic units (e.g. the Lofoten gneiss complex). The latter rock units are representative for middle and lower crust. While mafic rocks within underplated bodies and other mafic igneous rocks

provide a significant transient heat pulse, they have a low radioactive heat production. Assuming a constant heat production from the continental crust in basin modelling studies offshore Norway and other basins in the world will lead to considerable errors in the calculation of the temperature regime in sedimentary basins. Analysis of offshore and onshore well data is a fundamental step to obtain detailed input for heat flow and thermal gradients.

The present project aims at compiling lithogeochemical information on basement rocks in northern Norway with emphasis on characterizing the U, Th and K content (Fig. 1.1). Geophysical information such as seismic, aeromagnetic, and gravity data will, together with well penetrations of basement, provide a basis for extending this information below the offshore sedimentary basins. The Geological Survey of Norway (NGU) holds complete gravity and aeromagnetic databases from the whole of the Norwegian mainland and offshore areas in addition to detailed information on the mainland bedrock geology. The onshore-offshore geophysical interpretations will also be constrained by geochemical analysis and age dating of basement core samples obtained from offshore exploration wells.

Seismic velocity and seismic reflection patterns from offshore basement rocks will help in distinguishing between Caledonian nappe complexes and more massive Precambrian granites and gneisses. Hence a first order distribution of basement-related heat flow will be mapped.

An additional element of relevance to the heat flow in sedimentary basins is the structural relief of the basement; basement highs most likely act as focussing points for fluid that are being driven out from the overlying sediments. An element of the project will hence be to map the basement structure and to combine this with the mapped rock type distribution.

2 THERMAL LOGGING AND OVERVIEW OF VISITED DRILL HOLES IN 2006 AND 2007

Harald Elvebakk, NGU

2.1 Introduction

Two sondes were used for the thermal logging. The Water Quality Sonde (WQS) with high resolution sensors and the TCN sonde (Temperature, Conductivity, Natural gamma). Accuracy and resolution, see below.

WQS

Parameter	Range	Accuracy	Resolution	Time constant
Pressure	0 – 2000 dbar	0.05 %	0.0015 %	50 ms
Temperature	-1 – 50 °C	0.00 5 °C	0.001 °C	50 ms
Conductivity				
Salt water	0 – 64 mS/cm	0.005 mS/cm	0.001 mS/cm	50 ms
Fresh water	0 – 6400 µS/cm	1 µS/cm	0.1 µS/cm	50 ms
Oxygen	0 – 50 ppm	0.1 ppm	0.01 ppm	3 s
pH	0 – 14 pH	0.01 pH	0.001 pH	3 s
Redox potential	+/- 1000 mV	1 mV	0.1 mV	3 s
Nitrate, NO_3	0 – 100 mg/l			

TCN

Parameter	Range	Accuracy
Temperature	0 – 70 °C	0. 5 °C
Conductivity	0 – 50,000 µS/cm	+/- 2.5 % at 500 µS/cm
Natural Gamma	50 mm x 25 mm NaI scintillation crystal	

2.2 Båtsfjord

The Båtsfjord borehole was drilled to 800 m. The logging stopped at ~590 m because something was blocking the hole, probably stones. The borehole was first logged in 2006, but because of a planned reopening we wanted to check if the borehole still was open down to 590 m. In 2007 the borehole was logged with the water quality sonde one year after the first logging in 2006. By doing this we could check if the borehole conditions were changed and if the data were repeatable. Fig. 2.1 shows the borehole site Båtsfjordfjellet.

Figure 2.1. Temperature logging at Båtsfjordfjellet.

The borehole was still open down to ~590 m and the results from the WQS sonde are shown in Fig. 2.2. The figure shows logs from both 2006 and 2007. Because of problems with the oxygen sensor there are no data from this sonde in 2007. Natural gamma log is from 2006.

Fig. 2.3 shows the temperature logs and the gradients for 2006 and 2007. Small temperature changes can be seen in the upper 50 m and below 400 m. The upper temperature changes are caused by annual variations in the surface temperature. It seems to be a bit colder in 2007. Below 400 m there are small variations in the temperature both for the 2006 and 2007 measurements. The 20 m interval gradients clearly show these variations. The temperature seems to be a bit more stable in 2007.

The temperature gradient is low above 400 m, 4 –5 ^{o}C/km, but increase to 8 ^{o}C/km in the bottom of the hole (590 m). This could be caused by change in the thermal conductivity. The natural gamma log indicates rock boundaries at 240 m, 365 m and 475 m. It is interesting to notice that the water quality parameters, pH, Eh and O2 are changing at 365 m depth. The water conductivity is different in the upper 300 m for the 2006 and 2007 measurements. This is difficult to explain but it could be related to the use of cement during the drilling process.

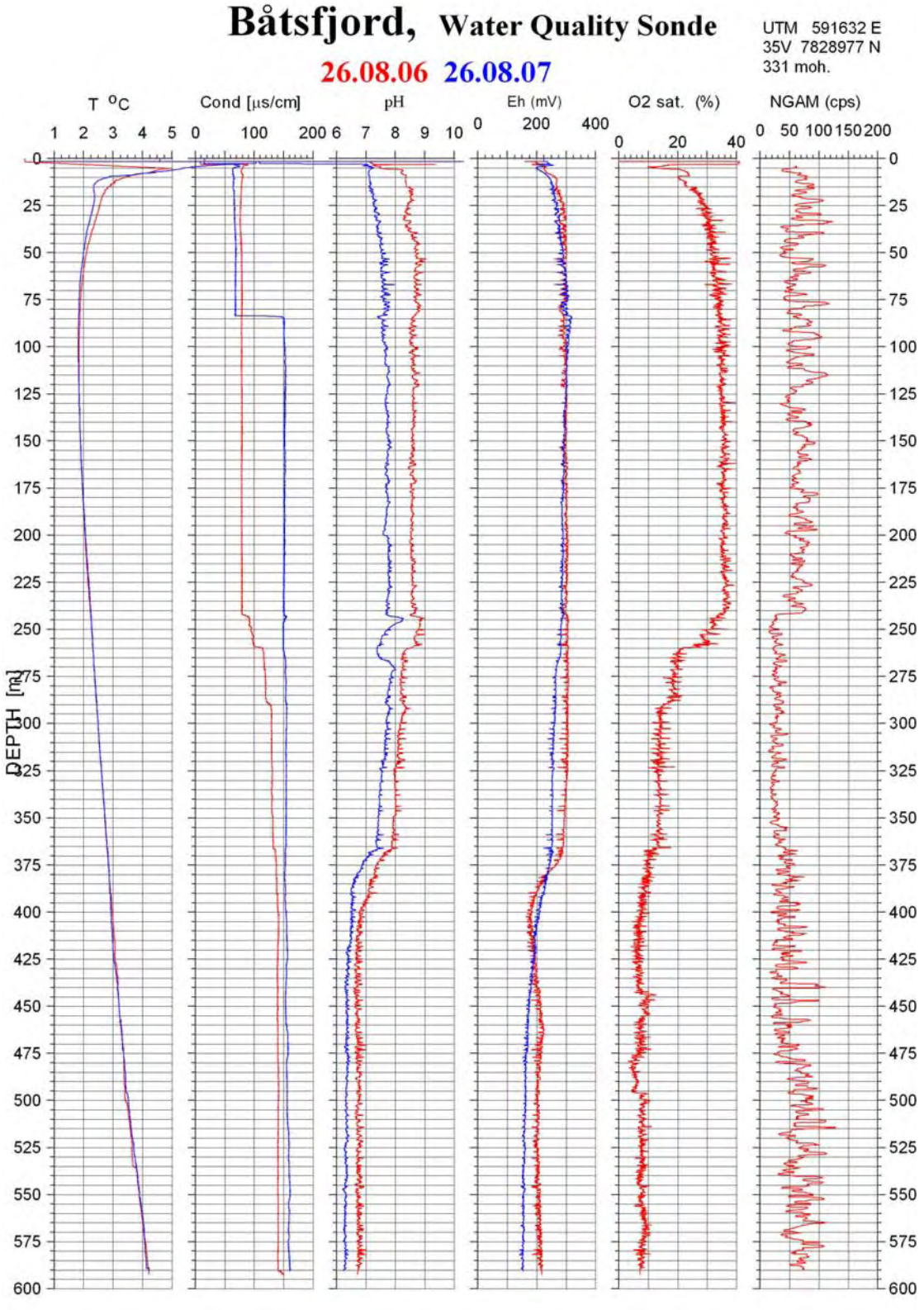

Figure 2.2. Båtsfjord borehole, logs from water quality sonde, 2006 (red) and 2007 (blue).

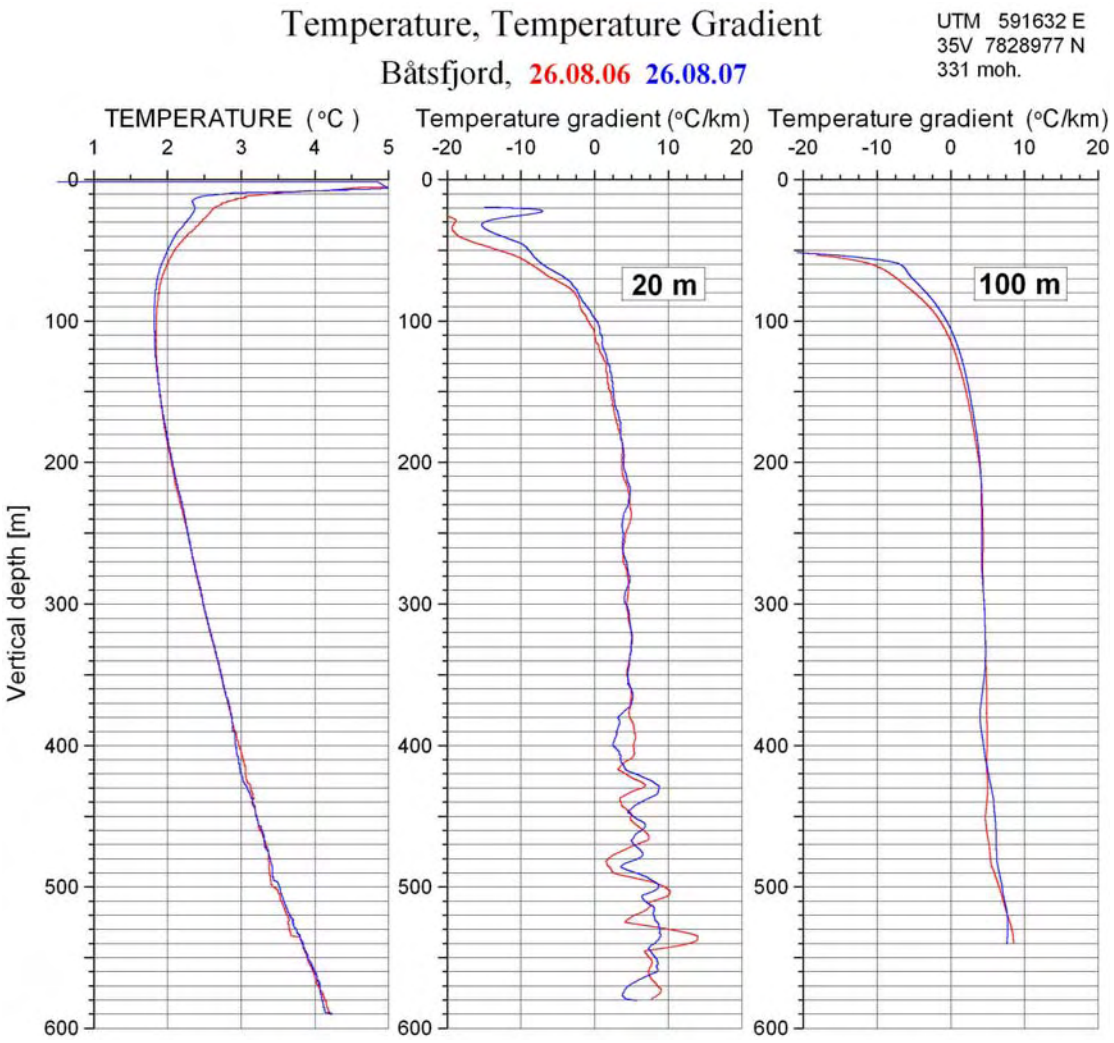

Figure 2.3. Båtsfjord borehole. Temperature and thermal gradient 2006 (red), 2007 (blue).

2.3 Bjørnevatn, Kirkenes

An old borehole close to the Bjørnevatn iron mine was logged in 2006. A part of the Bjørnevatn open pit mine is shown in Fig. 2.4. The figure also shows the borehole and the logging winch. Because of the small borehole diameter the TCN sonde was used.

Figure 2.4. The Bjørnevatn open pit (left) and borehole logging (right).

Fig. 2.5 shows the temperature log and the thermal gradient. The borehole was drilled to 634 m, but because of the deviation only 441 m (379 m vertical) were logged. The gradient is calculated using the vertical depth.

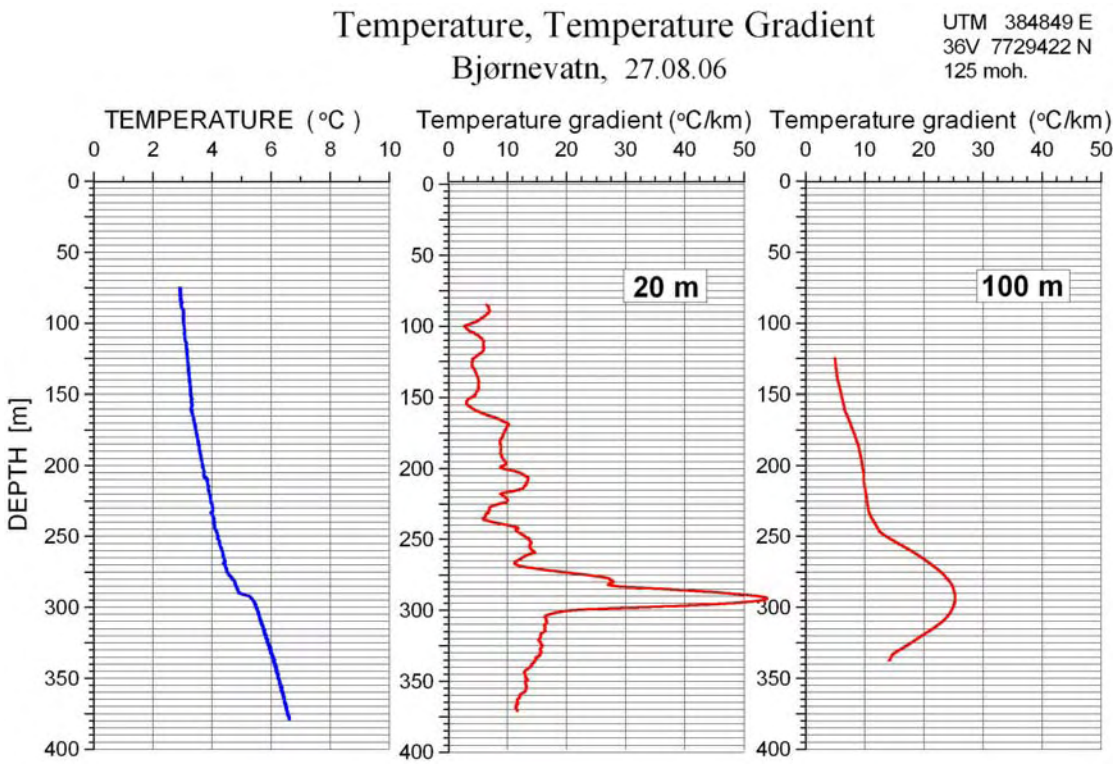

Figure 2.5. Bjørnevatn borehole. Temperature log and thermal gradient.

Fig. 2.6 shows temperature, water conductivity and natural gamma. In these logs the length of the borehole is used (not vertical depth). A change in the temperature level at 320 m can be caused by an open fracture with inflow of water. The water conductivity also changes at the same depth and the gamma log indicates a rock boundary.

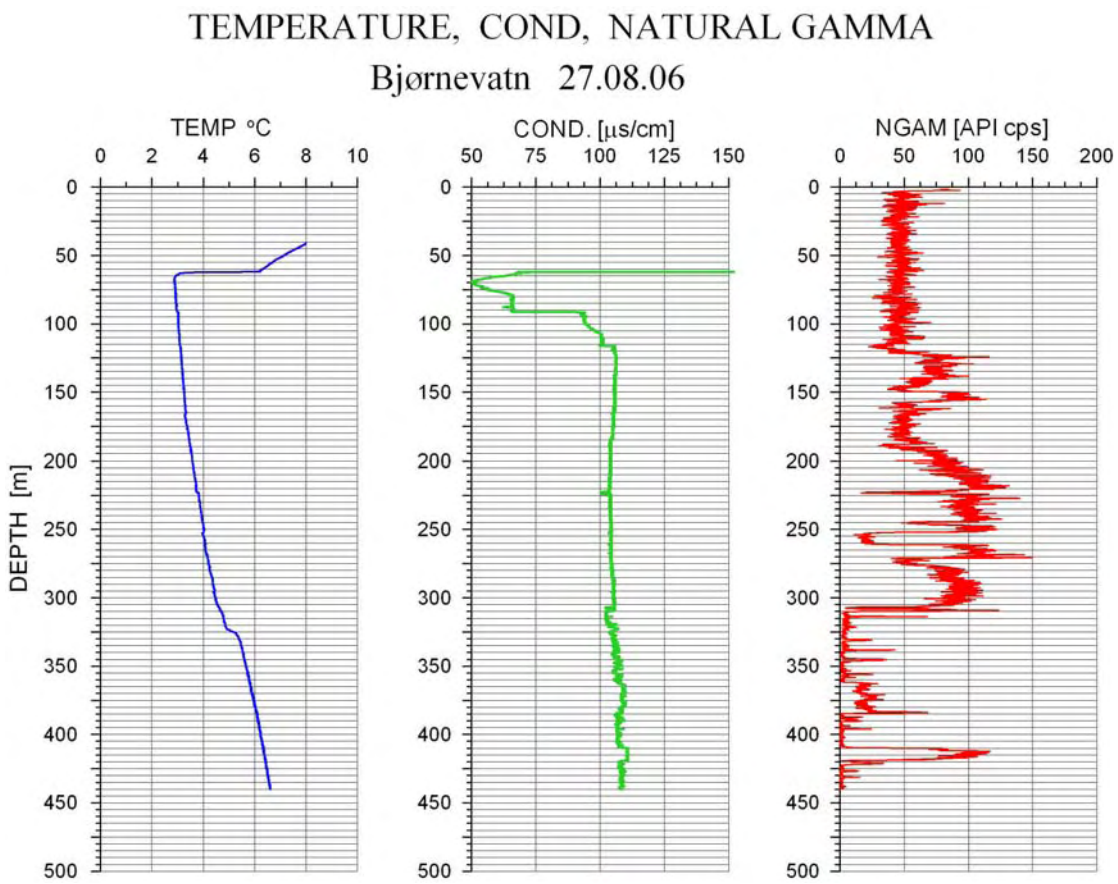

Figure 2.6. Bjørnevatn borehole. Temperature, water conductivity and natural gamma.

2.4 Borehole N340 Bidjovagge.

This old borehole is 653 m deep and situated about 4 km north of Bidjovagge Gruber (closed). The borehole was visited 27.08.07. It was blocked at 13 m depth and logging was not possible. In 2006 three other boreholes at Bidjovagge were visited, but they were all blocked at shallow depths.

3 HEAT FLOW DETERMINATIONS IN FINNMARK, PRELIMINARY RESULTS

Christophe Pascal, Harald Elvebakk, David Roberts, Anna Siedlecka, Bjørn Wissing, Odleiv Olesen & Jan-Reidar Skilbrei, NGU

3.1 Introduction

In the course of the summers 2006 and 2007 we logged two drillholes for heat flow calculations in Finnmark (Fig. 3.1). The first drillhole in Båtsfjordfjellet, Varanger Penninsula, is a vertical well drilled in the framework of the HeatBar project. The second one is an old mining well drilled in 1962 at the edge of the Bjørnevatn open pit. The details of the logging are reported in the previous chapter of the present report. In this chapter we present preliminary (i.e. uncorrected) heat flow determinations based on the measured temperatures and in-house thermal conductivity measurements and report briefly on the status of recent drilling at Vuoddašjav'ri, central Finnmark.

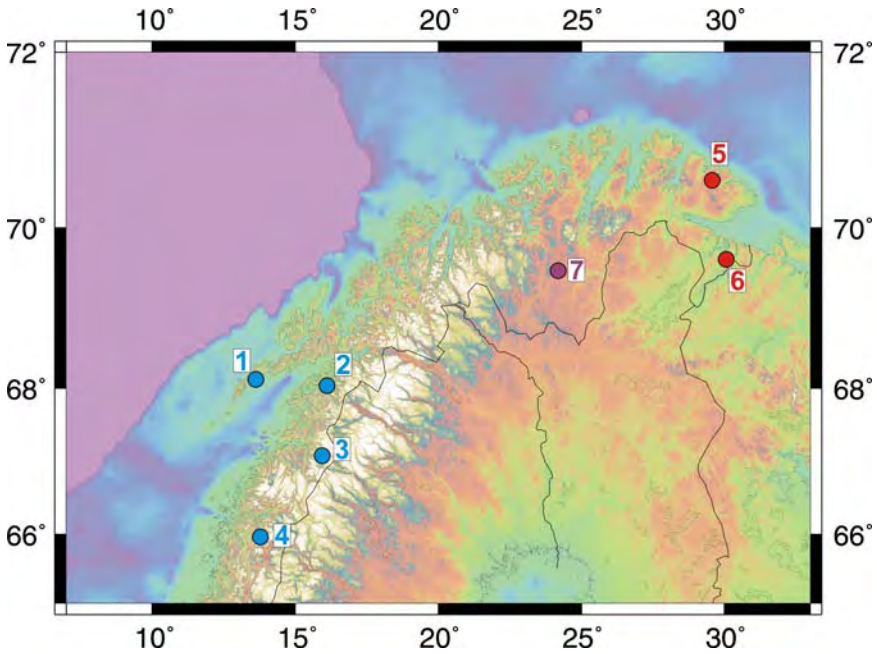

Figure 3.1. Heat flow sites in northern Norway: blue dots represent Kontiki wells (Olesen et al. 2007), red and purple respectively logged and awaiting for logging HeatBar wells. 1) Leknes, 2) Drag, 3) Sulitjelma, 4) Bleikvassli, 5) Båtsfjordfjellet, 6) Bjørnevatn and 7) Vuoddašjav'ri.

Table 3.1. Drillholes studied in the HeatBar project.

Site	UTM Zone	Coord. [1]	Elevation (m)	TD (m)	Max. dip (°)[2]
Bjørnevatn	36V	384849 7729422	125	384	48
Båtsfjordfjellet	35V	591632 7828977	331	592	90
Vuoddašjav'ri	35W	382955 7696752	340	720	90

[1]WGS84
[2]From horizontal.

3.2 Thermal conductivity measurements

Thermal conductivity of rock samples is measured with a transient method. A constant heat flow is induced to the top of the samples. The heat mechanism is radiation and the heat source, with a constant temperature of 300 ± 2ºC, is placed 10 mm above the top surface of the sample. The sample is insulated at all its other faces. Temperature is measured at the base of the sample. Thermal diffusivity (κ) is estimated from the temperature – time plot, and the thermal conductivity (k) is calculated from thermal diffusivity, measured density (ρ) and assumed specific heat capacity (c_p) of the sample using equation 3.1:

$$k = \rho c_p \kappa \qquad (3.1)$$

The theory of this method is described in Carslaw & Jaeger (1959) and Middleton (1993). Quality controls are carried out by measurements on the standard material Pyroceram 9606. The apparatus at NGU was improved in December 2005 and the error of the thermal diffusivity measurements is now within ± 5%.

3.3 Båtsfjordfjellet

The Båtsfjordfjellet borehole was drilled in December 2005 by the Finnish company Smoy. The borehole was cored from top to bottom and reached 800 m TD, additional information is given in Table 3.1. The borehole was logged for the first time August 26th 2006 and appeared to be blocked at ~592 m depth. We logged again the well August 26th 2007 three weeks before Smoy attempted to re-open and deepen the well. Unfortunately the borehole collapsed at ~620 m depth September 27th 2007.

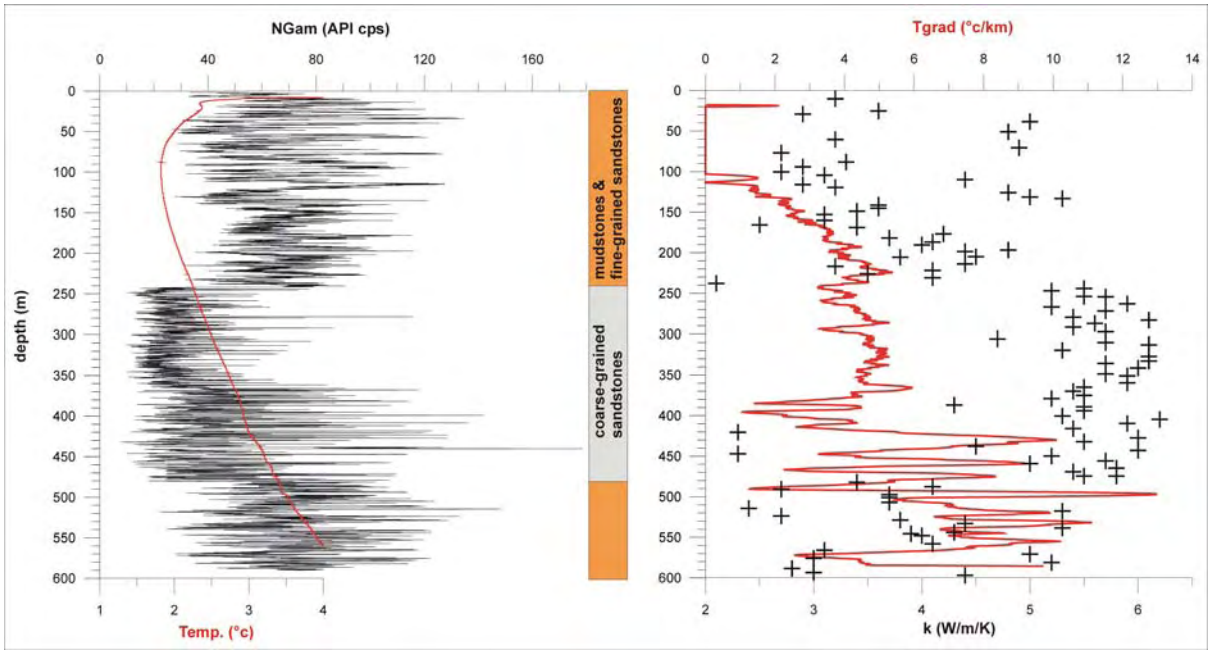

Figure 3.2. Båtsfjordfjellet: a) Temperature profile superimposed on the gamma log and simplified lithostratigraphic column. b) Computed thermal gradient (least-squared on a 10 m moving window) and measured thermal conductivies on core material.

Logged temperatures in the well appeared to be extremely low, reaching 4ºC at ~600 m depth and a minimum value of 1.75ºC at ~100m (Fig. 3.2). Accordingly the thermal gradient is also low varying from negative values above 100 m depth to 6 ºC/km on average in the deepest parts. In more detail strong variations of the thermal gradient (i.e. from 1 to 13 ºC/km, Fig. 3.2.) are seen below 400 m depth. These are probably the result of water circulation through small fractures and/or drastic changes in thermal conductivity.

Thermal conductivity values are extremely scattered and range from 2 to 6 W/m/K (Figs. 3.2 and 3.3a). Two groups of values can however be isolated. In the depth ranges 0-240 m and 480-600 m, conductivity values are scattered but fall most frequently in between 3 and 4 W/m/K (Fig. 3.2). In the depth range 240-480m, conductivity values are extremely high and better clustered around a mean value of 5.5 W/m/K. Those changes in thermal conductivity find their counterparts in changes in number of gamma countings and variations in bulk lithology (Figs. 3.2 and 3.3b). The upper and lower parts of the well penetrate mudstones and siltstones alternating with fine-grained sandstones whereas the central part exhibits almost exclusively medium to coarse grain sandstones. The higher content in radioactive elements and lower thermal conductivity of more shaly layers with respect to quartz-dominated ones explains the observed differences in the gamma log and measured thermal conductivities. Finally the extremely high thermal coductivities recorded for the sandstones of Båtsfjordfjellet is explained by their loss in porosity, conductivity values approaching the one of pure quartz (i.e. ~7 W/m/K, Brigaud & Vasseur 1989).

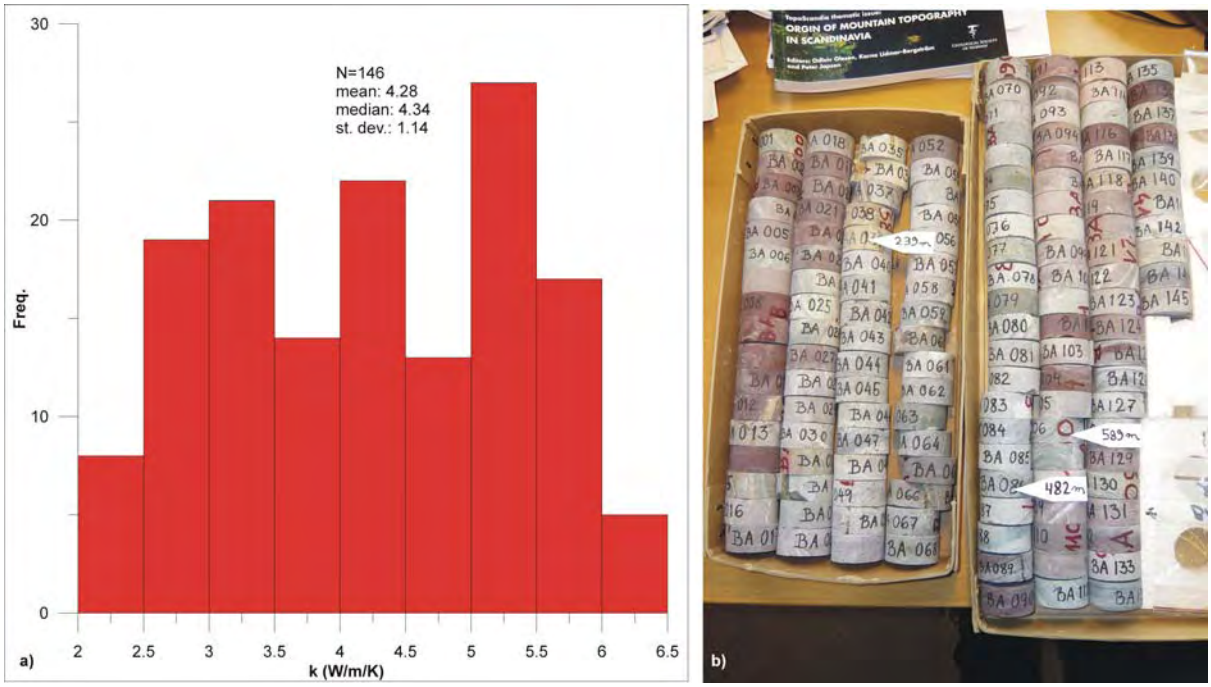

Figure 3.3. Båtsfjordfjellet a) Distribution of thermal conductivity values as measured from core material at different depths (see also Fig. 3.2). b) Core samples used for thermal conductivity measurements. Note the almost complete lack of reddish rocks (i.e. mudstones) between 239 and 482 m depth. Note as well coarser grain sandstones for the same depth interval.

In order to detect eventual departures from steady-state thermal conditions in the wells, we used the "Bullard Method" (Bullard 1939). The Bullard Method is based on the concept of thermal resistance expressed as:

$$R(z_i) = \Delta z_i / k_i \qquad (3.2)$$

where k_i is the thermal conductivity of the rocks located in the depth interval Δz_i.
Temperature at depth z can be written as a function of heat flow and thermal resistance (for a detailed description of the method see e.g. Beardsmore and Cull 2001):

$$T(z) = T_0 + \sum_{i=1}^{N} q(\Delta z_i).R(z_i) \qquad (3.3)$$

where $q(\Delta z_i)$ is the heat flowing through the depth interval Δz_i, N the number of depth intervals in between the surface and depth z and T_0 mean temperature at the surface.

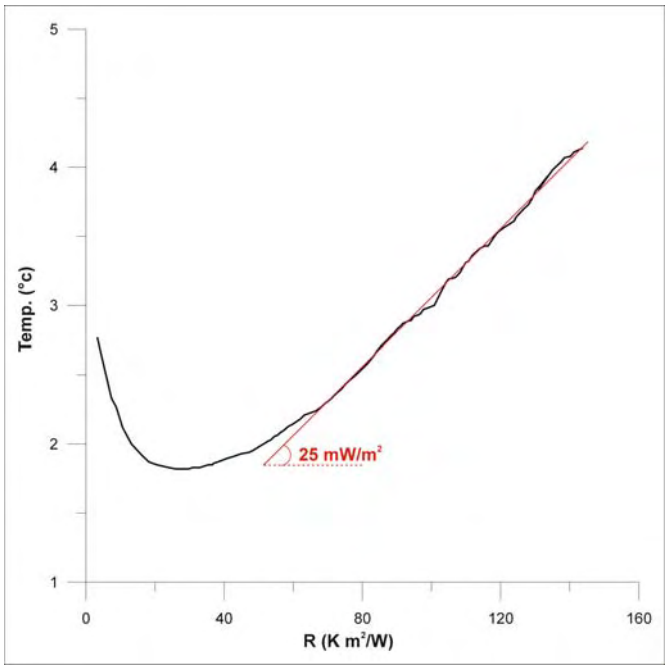

Figure 3.4. Båtsfjordfjellet: computed heat flow using the Bullard-plot technique, R represents thermal resistance.

Temperature versus thermal resistance plots are consequently called Bullard plots. From equation (3.2) it is implicit that if the heat flow is constant through the whole depth section sampled by the well (i.e. steady-state thermal conditions apply), the corresponding Bullard plot should be a line and the slope of the line should give the value of this constant heat flow.

However, if heat flow variations occur in the well (i.e. the thermal field is not in equilibrium whatever the reasons are) the corresponding Bullard plot is non-linear.
The obtained Bullard plot shows that heat flow increases gradually with depth and reaches a stable value of 25 mW/m^2 (Fig. 3.4). A more automated way to track eventual heat flow variations in the well and check its apparent stability for a given depth range consists in calculating series of regression lines (i.e. heat flow values), fitting successive sections of the obtained Bullard plot, and their respective correlation coefficients (i.e measure of the stability of the calculated heat flow value). Fig. 3.5 depicts the resulting heat flow/depth profiles while varying the number of successive points used to compute the regressions lines.

The fewer points are used in computing regression lines the more accurately are reflected short-wavelength heat flow variations (i.e. black profile in Fig. 3.5). In that specific case, we also note that drastic heat flow variations are associated with reduced quality in the determination of heat flow values (i.e. decrease in correlation coefficients, e.g. at ~440 m depth). Such cases correspond to even shorter wavelength variations in heat flow but with high amplitude (i.e. at ~440 m depth heat flow reaches up to 40 mW/m^2). Influx of "warm" meteoritic water following open fractures into the well is assumed to be the cause of these local anomalies. Conversely using more points to compute regression lines is equivalent to filter short-wavelength heat flow variations (i.e. red profile in Fig. 3.5). In the present case, it is important to note that (1) correlation coefficients are very close to one from ~150 m depth downwards, showing that calculated heat flow values are reliable, and (2) heat flow values remain reasonably stable by reaching 25 mW/m^2 below ~300 m depth.

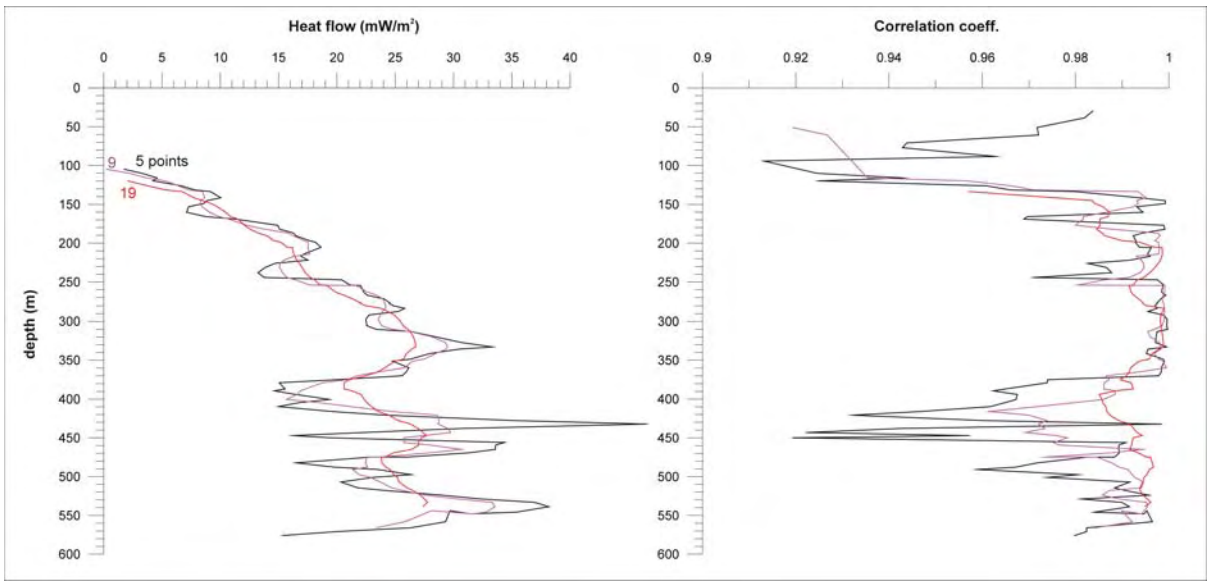

Figure 3.5. Båtsfjordfjellet: variation of heat flow vs depth. Heat flow profiles are constructed by computing series of regression lines for the Bullard plot showed in Fig. 3.4 and plotting their respective slopes vs depth. The number of points used to calculate regression lines for each heat flow profile is indicated as well as their respective correlation coefficients.

Finally, we estimated heat heneration following the empirical law from Rybach (1988):

$$HGen\ (\mu W/m^3) = 0.0145 * (GR(API)-5) \qquad (3.4)$$

where GR(API) represents gamma countings in American Petroleum Institute units.
The use of equation (3.4) remains valid here but one has to keep in mind that this relationship starts to break down when GR(API) > 150 API. The results suggest ~1 $\mu W/m^3$ in the more shaly layers decreasing to 0.2-0.4 $\mu W/m^3$ in the more sandy ones (Fig. 3.6). As expected the sedimentary rocks of Båtsfjordfjellet are relatively depleted in heat-producing elements. The basements rocks sourcing them were probably Archean to Early Proterozoic in age (see Chapter 5).

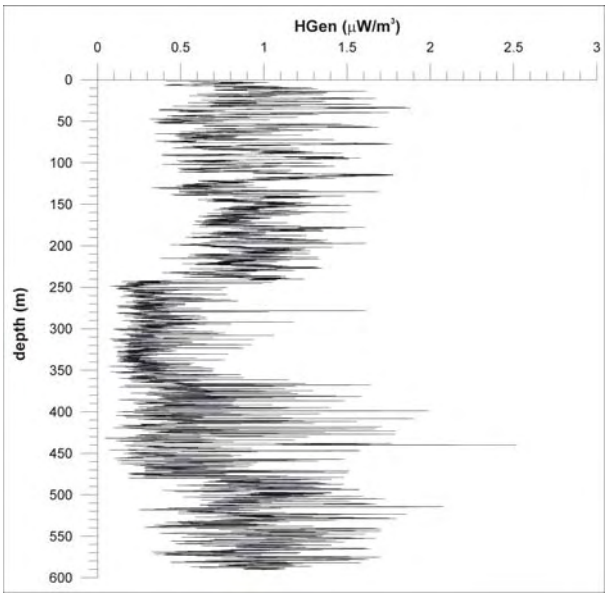

Figure 3.6. Båtsfjordfjellet: heat generation as derived from the gamma log.

3.4 Bjørnevatn

The Bjørnevatn 116 well was drilled down to ~630 m (~520 TD) in 1962. It is located ~70 m away from the open pit. The well could be logged down to ~385 m TD only. Core material was not available for this specific well neither in Bjørnevatn nor at NGU in Løkken. We collected hand samples representative of the main lithologies of the area (i.e. Bjørnevatn gneiss, sericitic quartzite, diabase and ore) and measured their respective thermal conductivities (Table 3.2). We used conductivity median values and the available geological log in order to build an a priori thermal conductivity model for the rocks encountered in the drillhole.

Table 3.2. Thermal conductivity (in W/m/K) of the main lithological units of the Bjørnevatn open pit.

Lithology	Number of samples	Mean k	Median k	Std.
Bjørnevatn gneiss	5	3.3	3.5	0.46
Sericitic quartzite	4	3.1	3.2	0.28
Diabase	5	2.7	2.7	0.17
Ore	6	5.7	5.8	0.39

Both the temperature log and the calculated thermal gradient show sharp variations (Fig. 3.7). These variations are clearly associated with water circulation through fracture zones and less frequently lithological boundaries (i.e. sharp change in thermal conductivity) as suggested by a quick look to the other logs (gamma, water conductivity and geological logs). More surprising is the violent increase in thermal gradient (i.e. up to 80 ºC/km) at ~290 m depth. This spike in the geotherm is preceeded by another but less pronounced spike.

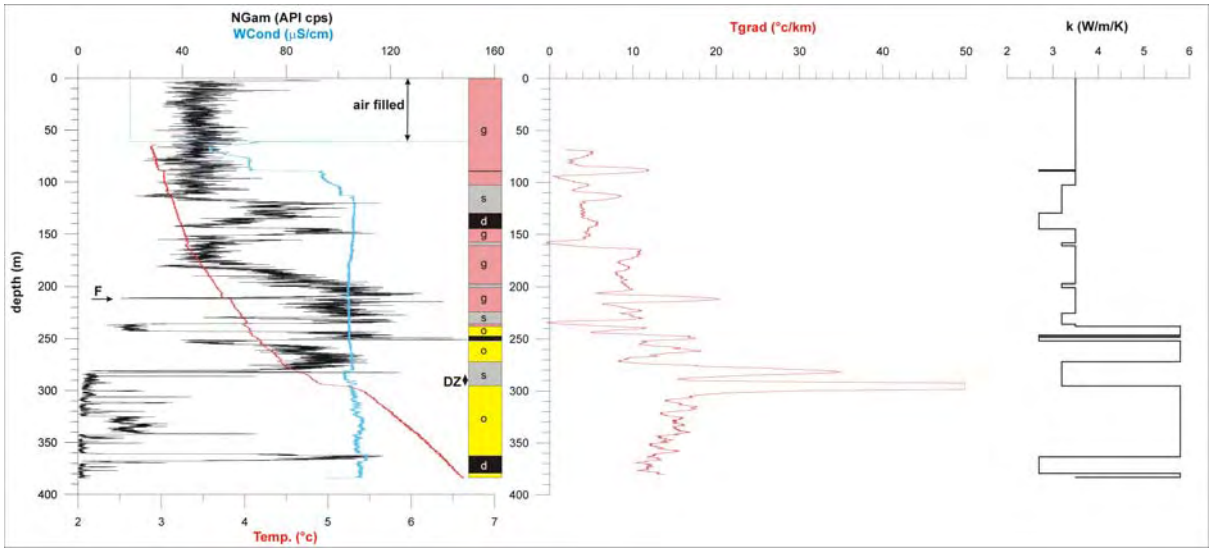

Figure 3.7. Bjørnevatn: a) Temperature profile superimposed on gamma and water electrical conductivity logs and simplified lithostratigraphic column (g = Bjørnevatn gneiss, s = sericitic quartzite, d = diabase, o = ore, F= fracture, DZ= deformation zone). Note that, in general, highs and lows in the gamma log correspond to the presence of diabase dykes and ore bodies respectively. b) Computed thermal gradient (least-squared on a 10 m moving window). c) Thermal conductivity model.

They apparently correspond to an increase in temperature of ~1ºC in 30 m following two steps in the temperature log. Both the gamma and the water conductivity logs point towards a marked lithological boundary at corresponding depths. In turn the geological log suggests a complex zone of polyphased deformation involving breccia and different kinds of minerals before reaching the boundary between a quartzite bed and an ore body (Fig. 3.7). We suggest that the sharp changes in the geotherm at ~270-300 m depth are caused by a combination of reduced thermal conductivity inside a major shear zone (not included in the a priori conductivity model) and water flowing through open fractures.

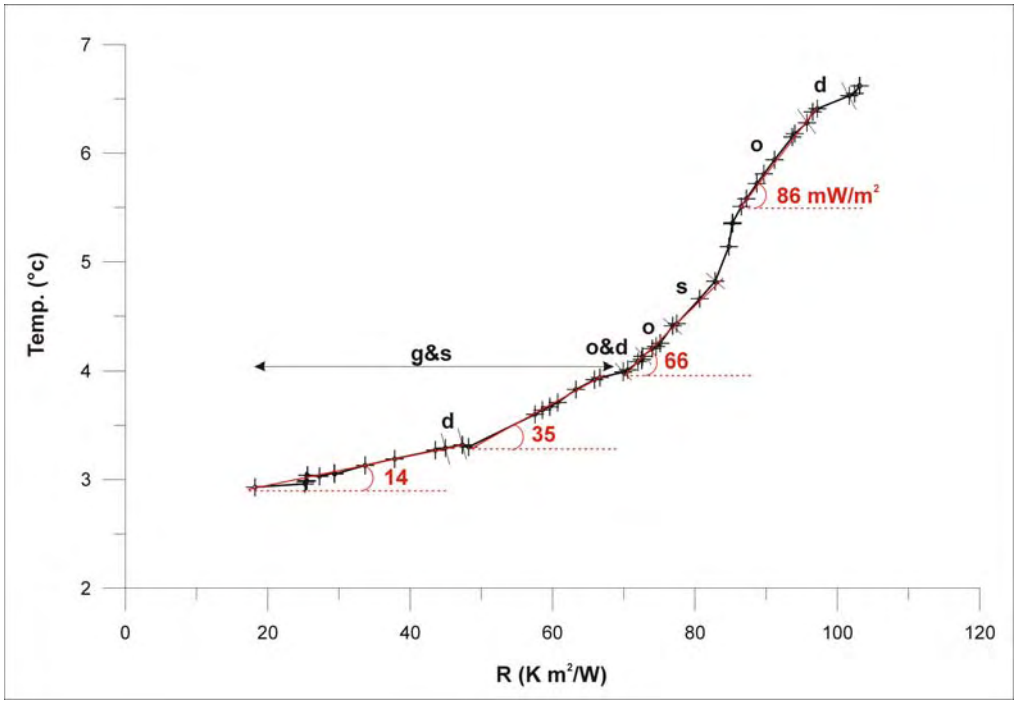

Figure 3.8. Bjørnevatn:computed heat flow using the Bullard-plot technique, R represents thermal resistance. Main lithologies for different intervals are indicated: d = diabase, g = gneiss, s = sericitic quartzite, o = ore.

Based on the data described above we tentatively used the Bullard method in order to determine heat flow values for the Bjørnevatn 116 drillhole. Our analysis suggests a stepwise increase in heat flow from 14 to 86 mW/m^2 (Fig. 3.8) when moving downwards from 60 to 380 m depth. This step-like pattern seems to be dictated by the already noticed sharp offsets in temperature induced by groundwater flow in the well. We proceeded with a similar automated analysis of heat flow as described previously. Unfortunately the sharp changes in the geotherm together with the relatively scarce thermal conductivity model makes the resuls too much influenced by local anomalies and in particular by the violent change in thermal gradient at ~270-300 m (Fig. 3.9). In the present case a more traditional way to treat the Bullard plot by picking by eye the best-fitting regression lines is obviously preferable.

An increase in heat flow downwards is expected due to the expected influence of (palaeo)climatic changes. However the magnitude of the variation appears to be extremely high (i.e. up to 72 mW/m^2, Fig. 3.8). The high thermal conductivity of ore as compared to the surrounding rocks might explain part of the high heat flow, determined at the depth of the deepest ore body encountered in the logged depth range. Heat has the tendency to travel through the less resistive (i.e. most conductive) layers of the Earth's crust, especially when those are close to vertical (i.e. "cheminee effect") like in the present case. Alternatively, because thermal conductivity of ore is significantly variable (Table 3.2), presumably as a function of iron content, we might have overestimated the heat flow value for the lowermost ore body. This seems to be somehow supported by the very last break in slope observed for the Bullard plot. Our preferred heat flow value would be the one determined at relatively deep levels in the well involving different types of lithologies (i.e. 66 mW/m^2, Fig. 3.8). In

this latter case, the consistency of the Bullard plot slope in the context of highly variable thermal conductivities adds confidence to the quality of the result.

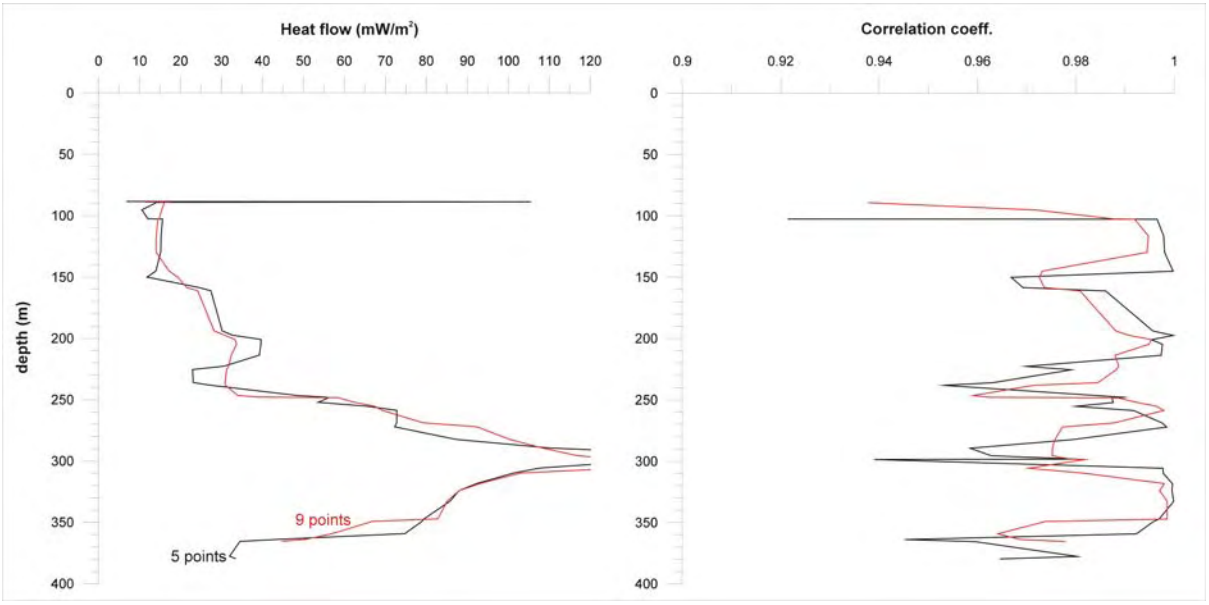

Figure 3.9. Bjørnevatn: variation of heat flow vs depth. Heat flow profiles are constructed by computing series of regression lines for the Bullard plot showed in Fig. 3.8. and plotting their respective slopes vs depth. The number of points used to calculate regression lines for each heat flow profile is indicated as well as corresponding correlation coefficients.

Similarly to the Båtsfjordfjellet drillhole we estimated heat generation from the gamma log (Fig. 3.10). As expected for these Archean rocks, heat generation is low, in the range of 0.6-0.8 $\mu W/m^3$ for gneisses, dropping down to 0 $\mu W/m^3$ for some of the ore bodies and, in general, higher than 1 $\mu W/m^3$ for sericitic quartzites and diabase intrusions. Noteworthly, diabase appears to be the most radiogenic rock in Bjørnevatn.

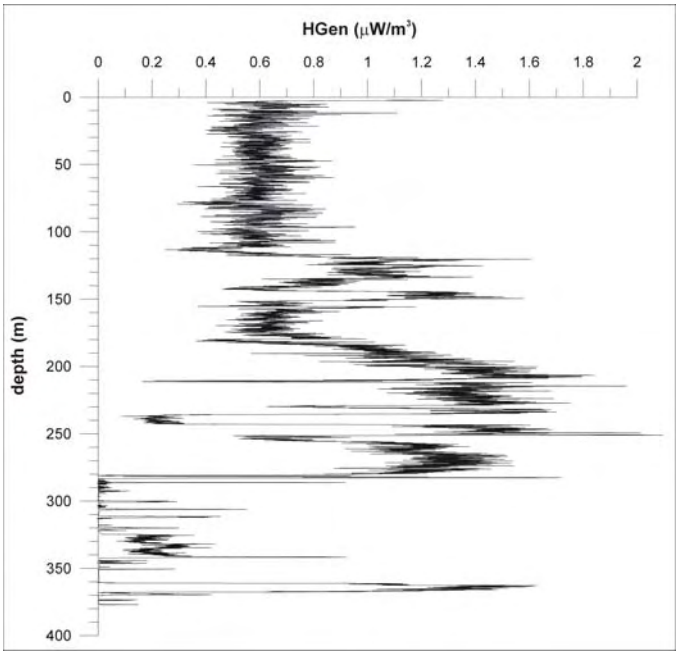

Figure 3.10. Bjørnevatn: heat generation as derived from the gamma log.

3.5 Recent drilling at Vuoddašjav'ri

In the framework of the HeatBar Project Smoy drilled a new well near the Vuoddašjav'ri lake in central Finnmark (Fig. 3.1.). Drilling took place from May 14th until June 15th 2008 (Fig. 3.11). The well was drilled vertically in Archean gneisses with a target depth of 800 m. Thanks to the good rock quality, no major problems were encountered during drilling except at ~720 m where the unexpected presence of a thick clay zone (presumably fault gouge) forced the decision to stop drilling operations. Core recovery is good and the cores are currently stored in Løkken and will be sampled for conductivity measurements this autumn. The drillhole will be logged by spring 2009.

Figure 3.11. Drilling by the Vuoddašjav'ri Lake in central Finnmark (May 08).

3.6 Summary and future work

We reported preliminary heat flow determinations from Båtsfjordfjellet and Bjørnevatn eastern Finnmark. For Båtsfjordfjellet a stable value of 25 mW/m^2 was found in the deepest parts of the well. Obviously a strong paleoclimatic signal is superimposed on the steady-state value. Heat flow values derived for the Bjørnevatn drillhole are much more variable with depth (i.e. from 14 to 86 mW/m^2). Our preferred value for Bjørnevatn is 66 mW/m^2. However, we anticipate that subvertical ore bodies encountered in the well strongly distort the local geothermal field by focussing heat.

Our remaining tasks for the coming months will be:

- to correct from paleoclimatic, topographic and structural effects the obtained heat flow values at Båtsfjordfjellet and Bjørnevatn (October-November 2008);
- to log the cores the Vuoddašjav'ri drillhole and measure thermal conductivity at relevant depths form the hole (December 2008-February 2009);
- to log the Vuoddašjav'ri well (May-June 2009).
- to calculate heat production in the wells from ICP-MS data (January 2009).

4 RADIOGENIC HEAT PRODUCTION

Trond Slagstad, NGU

4.1 Introduction

Radiogenic heat production rates determined on rock samples from the Earth's surface, although biased towards upper crustal rocks, provide key input and constraints on thermal models of the lithosphere. A number of studies have shown lithology to be the main source of variation in radiogenic heat production rate (Kukkonen & Lahtinen 2001), but factors such as tectonic setting, tectonometamorphic history and major element composition may also play a role. Some studies indicate that heat production rates are relatively uncorrelated with the age of a particular rock type or geological province (e.g. Kukkonen & Lahtinen 2001), but there are also examples to contrary (e.g. McLaren et al. 2003).

4.2 Sources of heat production data

The heat production rate of individual samples is calculated following Rybach (1988), based on the samples' K, U and Th concentrations, and density. The chemical data used to calculate heat production come from various sources, summarised in Table 4.1 The majority of the samples have been analysed by XRF and LA–ICP–MS, thus a complete set of major and trace element data exists for each of these samples. The analytical procedure, detection limits, accuracy and precision of the LA–ICP–MS analyses are described in Flem et al. (2005). With regard to calculating heat production, K concentrations are from the XRF data whereas U and Th concentrations are from the LA–ICP–MS data. The remaining samples have been analysed by γ-ray spectrometry, thus for these samples we have no chemical information outside the concentration of heat producing elements. The analytical procedure, detection limits, accuracy and precision of the γ-ray spectrometry method are described by Raade (1973) and Killeen & Heier (1975). For several geological units, heat production data based on both XRF/LA–ICP–MS and γ-ray spectrometry exist. Average heat production rates for such units are similar regardless if they are based on the older γ-ray data or more modern XRF/LA–ICP–MS data, suggesting that the quality of the former are good. The densities of the Lito-project samples have been determined using Archimedes' principle by weighing the samples in air and immersed in water. Densities of the other samples have been assigned based on lithology, and are, where available, similar to those assigned by the original authors.

Table 4.1. Sources of heat production data.

Source	No.	Analytical method
LITO-project	2050	XRF, LA–ICP–MS
LITO-project, Finnmark, awaiting analysis	350	XRF, LA–ICP–MS
Various NGU samples	623	XRF, LA–ICP–MS
Killeen & Heier (1975)	629	γ-ray spectrometry
Raade (1973)	967	γ-ray spectrometry
Ormaasen (1976)	102	γ-ray spectrometry

4.3 Radiogenic heat production rates of Norwegian bedrock

As stated in the introduction, a number of factors, of which lithology, tectonic setting, tectonometamorphic history and age are the most obvious, may influence the heat production and heat flow of a geologically distinct terrain. Furthermore, the work presented here is part of a larger effort to enhance our understanding of the geological and thermal structure of the continental margin of Norway (and the Baltic Shield). This means that heat production values must be assigned to geological terrains onshore that can be correlated offshore onto the continental margin using seismic or potential field data. With these objectives in mind, I have previously presented and discussed the heat production data in reference to specific geological units or terrains, subdivided based on lithology, tectonic setting, tectonometamorphic history and age (Figs. 4.1 and 4.2, Table 4.2, Olesen et al. 2007).

4.4 Summary of previous work

The already extensive, and growing, geochemical database from Norwegian bedrock allows for comprehensive investigations into the factors that control the distribution of the heat producing elements. Since the purpose of this chapter is to characterise the heat production of the main geological provinces in Norway, a major part of this discussion focuses on average heat production rates obtained from a variety of rock types that in some cases formed at different times and in different tectonic settings. However, in general the geological provinces delineated here are dominated by a small number of lithologies that display rather modest geological variation (i.e., composition, age, metamorphic grade, tectonic setting) to make such a discussion meaningful. Because granite (*sensu lato*) is the main host for the heat producing elements, the heat production of Norwegian granites is discussed in particular, emphasising the relationship between the tectonic setting in which the granite formed and its heat production rate.

4.5 Heat production vs. lithology, composition and tectonic setting

4.5.1 Lithology and chemical composition

Lithological variation is the primary factor controlling the distribution of heat production in the crust. In general, granitic rocks have relatively high heat production whereas intermediate and mafic lithologies produce less heat, however, in reality heat production within the same lithology may vary by an order of magnitude or more. To facilitate the discussion of heat production and its dependence on lithology, I have subdivided the samples for which we have a complete geochemical data set (XRF and LA–ICP–MS) into 4 lithological groups. 'Metasedimentary rocks' encompass arkose, quartzite, mica schist, phyllite and greywacke; 'Metamafic rocks' include gabbro, amphibolite, diorite and greenstone/-schist; 'Granite and granitic gneiss' and 'Granodiorite and granodioritic gneiss' are self-explanatory. As expected, the mafic rocks yield the lowest heat production with an average of 0.74 $\mu W/m^3$ and the granitic rocks the highest heat production with an average of 2.95 $\mu W/m^3$. The granodioritic and metasedimentary rocks yield similar, intermediate heat production with averages of 1.54 and 1.55 $\mu W/m^3$, respectively. These values are as expected, and the variation within each lithological group in relation to chemical composition is perhaps more interesting. Fig. 4.3 shows heat production vs. SiO_2, Fe_2O_3 and total rare earth element (REE) content for the different lithological groups. SiO_2 and Fe_2O_3 represent the samples' major element composition and reflect the mineralogical composition of the samples, whereas total REE represents trace elements mainly hosted by accessory phases including zircon and monazite, which are also the main hosts of the heat producing elements (e.g. Bea 1996).

Table 4.2. Simplified geological history and heat production rates of geological provinces in Norway (from Kontiki report).

	Geological province	n	Age (Ma)	Lithology	Tectonic setting	Tectonometamorphic history	Heat production rate ($\mu W/m^3$)		Heat flow (mW/m^2)	
							Area wtd. mean[1]	Median ±1σ	Mean ±1σ (n)	Median
1	Archaean gneisses	95	3000–2500	Dominantly tonalitic to granitic gneisses		Early Proterozoic (c. 2.0–1.8 Ga) amphibolite- to granulite-facies metamorphism.	1.25	0.81 ± 1.48	38 ± 8 (2)	38
2	Proterozoic gneissic rocks									
2a	Karasjok-Kautokeino greenstone belts, NE Norway	n.d.	2100-2000	Tholeiitic metabasalts, amphibolites and interlayered metasedimentary rocks	Continental rifting and oceanic subduction	Metamorphosed under greenschist- to amphibolite-facies conditions during obduction onto the Karelian craton at c. 1.9 Ga.	n.d.	n.d.	24 (1)	24
2b	Palaeoproterozoic gneisses	17	2000–1900	Garnet-quartz-feldspar paragneiss and hypersthene-plagioclase orthogneiss	Deposition in continental back-arc basin	High-grade metamorphism during continent-continent collision at c. 1900 Ma	1.42	0.54 ± 1.44	38 ± 3 (16)	38
2c	Transscandinavian Igneous Belt (TIB)	571	1810–1770	Alkali-calcic to calc-alkaline quartz monzonites to granites	Active continental margin, back-arc extension	Deformation and metamorphism at c. 1.46–1.42 and 1.0 Ga in SW Sweden. Variable Caledonian effects in NW Norway at c. 420 Ma.	2.57	2.57 ± 2.03	38 ± 8 (4)	38
2d	Sveconorwegian Province, S Norway	385	1500–1000	Tholeiitic to calc-alkaline, intermediate to felsic, metavolcanic and –plutonic suites	Active continental margin and continental back-arc.	Local crustal reworking at 1.26–1.16 Ga. Continent-continent collision and associated medium- to high-grade metamorphism at c. 1.0 Ga. Very low-grade Caledonian metamorphism at c. 400 Ma in western areas.	1.76	1.73 ± 1.45	43 ± 8 (25)	45
2e	Western Gneiss Region, W Norway	332	1750–1000	Dominantly tonalitic to granitic gneisses	Active continental margin	Sveconorwegian and Caledonian high-grade metamorphism at c. 1000 and 400 Ma, respectively.	1.36	1.41 ± 0.82	42 ± 9 (8)	41
3	Lofoten anorthosite-mangerite-charnockite-granite (AMCG) complex	130	1800–1790	Mangerite, smaller volumes of gabbro, anorthosite, charnockite and granite	Related to TIB 1 magmatism	Crystallised under low-P granulite-facies conditions. No significant later metamorphic events.	0.65	0.61 ± 0.32	n.d.	n.d.
4	Post-Sveconorwegian granites, S Norway	473	930–920	Dominantly granite, locally grading to diorite	Extensional, post-tectonic magmatism	Generally no significant metamorphic overprinting.	4.61	3.92 ± 2.54	58 ± 17 (12)	59
5	Egersund anorthosite-mangerite-charnockite (AMC) complex	47	930	Massive anorthosite, lesser volumes of leuconorite, mangerite and charnockite	Extensional, post-tectonic magmatism	Very low-grade Caledonian metamorphism at c. 400 Ma.	0.57	0.71 ± 0.42	21 (1)	21
6	Caledonian thrust-sheets									

	Geological province	n	Age (Ma)	Lithology	Tectonic setting	Tectonometamorphic history	Heat production rate ($\mu W/m^3$)		Heat flow (mW/m^2)	
							Area wtd. mean[1]	Median ±1σ	Mean ±1σ (n)	Median
6a	Late Proterozoic to Palaeozoic metasedimentary and metamafic rocks	561	500–450	Metagreywacke, phyllite, mica schist, lesser volumes of marble and greenstone.	Passive margin sequences. Greenstones formed in oceanic arc / back-arc.	Low- to high-grade metamorphism during the Caledonian orogeny at c. 450–400 Ma.	1.47	1.40 ± 1.39	48 ± 8 (12)	49
6b	Caledonian intrusive rocks	167	480–430	Dominantly calc-alkaline diorite, tonalite, granodiorite and granite. Minor trondhjemitic intrusions.	Active continental margin.	Variable overprinting during the Caledonian orogeny at c. 430–410 Ma.	1.85	1.74 ± 1.85	66	66
6c	Seiland igneous province	n.d.	570–560	Gabbro, lesser volumed of ultramafic rocks and intermediate granitoid rocks.	Intracontinental rift.	Variable overprinting during the Caledonian orogeny at c. 420 Ma.	n.d.	n.d.	n.d.	n.d.
6d	Precambrian gneissic rocks	35	1690–950	Syenitic to monzonitic gneisses, anorthosite-mangerite-charnockite-granite suites	Active continental margin. AMCG suite formed in intraplate setting (?)	Late Sveconorwegian, high-grade metamorphism at c. 930 Ma. Variable, but locally high-grade metamorphism at c. 450 Ma.	2.01	1.70 ± 1.78	41 ± 11 (4)	43
6e	Neoproterozoic metasedimentary rocks	48	1000–500	Quartzitic to arkosic sandstone, mica schist, pelite and volumetrically subordinate carbonate	Continental shelf	Variable high- to low-grade Scandian and pre-Scandian metamorphism in Finnmark. Low-grade overprinting in Lillehammer during the Scandian phase at c. 430-400 Ma.	1.35	1.31 ± 0.82	43 ± 6 (4)	42
7	Devonian sedimentary rocks	15	400–390	Fluvial sandstones, conglomerate, breccia	Post-orogenic extension	No metamorphic overprinting.	1.33	1.23 ± 0.47	n.d.	n.d.
8	Cambro–Silurian sedimentary rocks	37	540–420	Marine shales, carbonates, sandstones	Epicontinental basin, later foreland basin	Low-grade metamorphism and deformation during the Caledonian orogeny at c. 420 Ma; local contact metamorphism during formation of Oslo rift at c. 300–280 Ma.	1.89	1.56 ± 1.45	48 ± 8 (6)	51
9	Oslo Rift	1044	300–280	Tholeiitic basalts, monzonite, syenite and granite	Intracontinental rift.	No metamorphic overprinting.	2.93	2.50 ± 1.64	45 ± 8 (4)	46

See Kontiki report for details and references.

[1]Area-weighted heat production of all map units classified within the particular geological province.

n.d. = not defined.

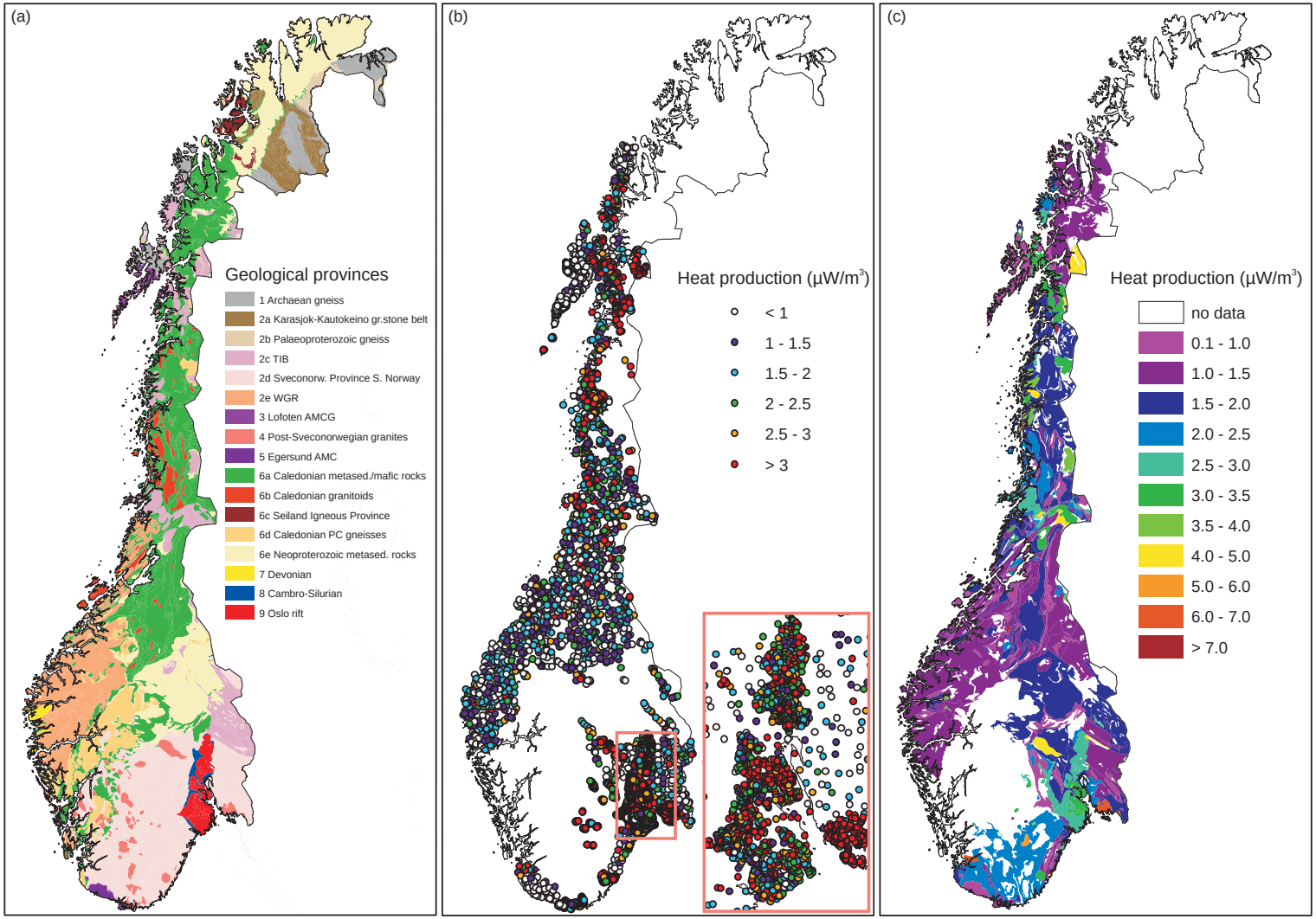

Figure 4.1. (a) Simplified geological map, modified after Sigmond (1998). (b) Heat production data. (c) Average heat production rates for geological units where data are available (from Kontiki report: Olesen et al. 2007).

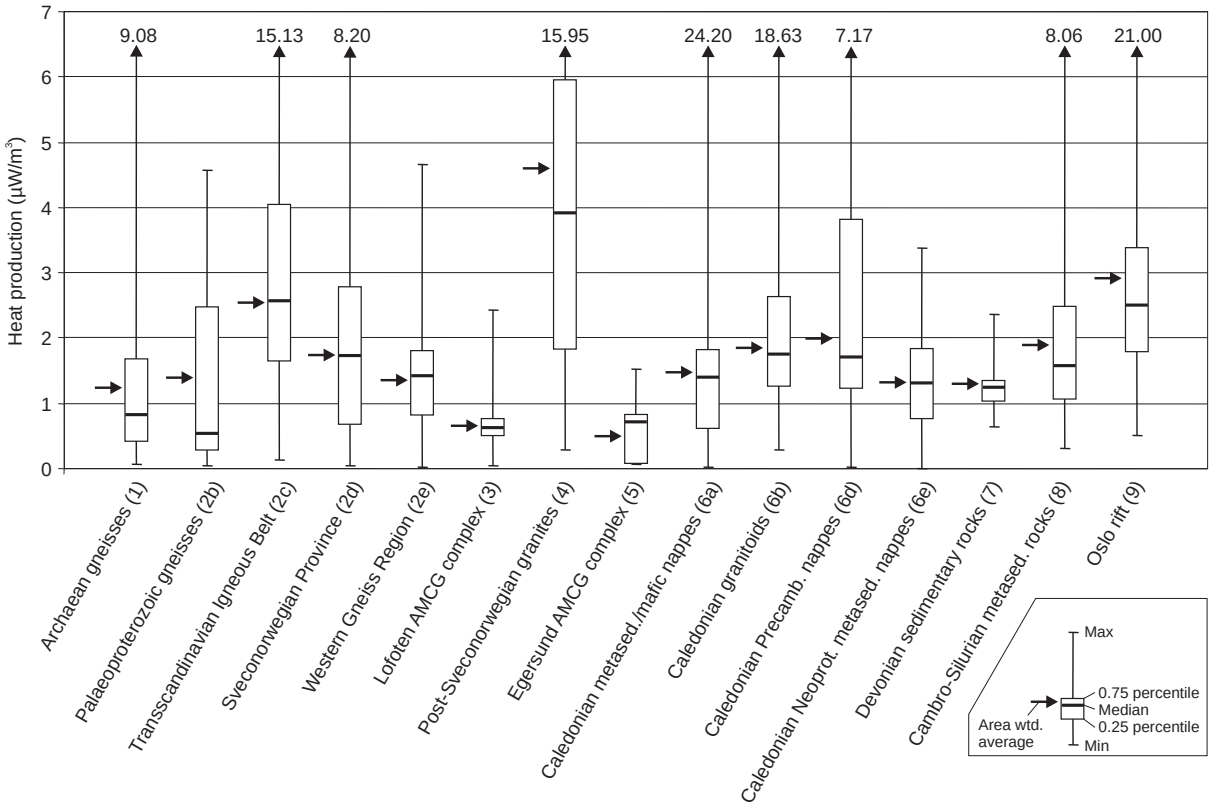

Figure 4.2. Heat production data from geological units presented in Table 4.2. and Fig. 4.1.

The metasedimentary rocks show a small increase in heat production with increasing SiO_2 at low SiO_2, then a gentle decrease (Fig. 4.3a). The trend is opposite with respect to Fe_2O_3 (Fig. 4.3e). In contrast the other 3 groups, consisting of magmatic rocks and orthogneisses, display increasing heat production with increasing SiO_2 (Figs. 4.3b-d) and vice versa with respect to Fe_2O_3 (Figs. 4.3f-h). These variations reflect different mechanisms controlling the mineralogical and major element composition of sedimentary and magmatic rocks (Kukkonen & Lahtinen 2001). The composition of sedimentary rocks partly reflects their source, resulting in correlations that are similar to those observed in magmatic rocks, and partly sedimentary sorting due to variation in the grain size and density of different minerals. Mica-rich rocks such as schist and phyllite represent low degrees of sedimentary sorting whereas quartz-rich rocks such as arkose and quartzite represent high degrees of sorting. Since U- and Th-bearing minerals are commonly hosted by micas, sedimentary sorting results in an inverse correlation between heat production and degree of sorting. The variation in heat production with SiO_2 and Fe_2O_3 in the metasedimentary rocks reflects both these processes. Between 45 and 60 wt.% SiO_2, heat production increases with increasing SiO_2. The rocks in this range include mica schist and phyllite, representatives of poorly sorted sediments, and the variation in heat production most likely reflects that of the source. Rocks with >60 wt.% SiO_2 consist of mica schist and phyllite at low SiO_2 and arkose and quartzite at high SiO_2, representing increasing degrees of sorting, resulting in an inverse correlation between SiO_2 and heat production. The other lithological groups represent magmatic rocks of mafic to intermediate ('Metamafic rocks'), intermediate to felsic ('Granodioritic rocks'), and felsic ('Granitic rocks') composition. The increase in heat production with SiO_2 and opposite for Fe_2O_3 is consistent with magmatic processes where low degrees of partial melting and/or high degrees of fractionation result in high SiO_2/low Fe_2O_3 melts with high incompatible

element (including U, Th) contents and vice versa. At very high SiO_2 and low Fe_2O_3, the relationship breaks down due to crystallisation of accessory phases that deplete the residual melt in incompatible elements; thus, further fractionation and concomitant increase and decrease in SiO_2 and Fe_2O_3, respectively, does not lead to increased levels of elements which were incompatible earlier in the fractionation process.

Figures 4.3i-l show how heat production varies with total REE content. In most rocks, REE are hosted by accessory phases and REE content may therefore be used as a proxy for the amount of accessory phases in a rock. All rock types show a relatively well-defined positive correlation between total REE content and heat production, supporting the general consensus that the heat producing elements are hosted dominantly by accessory phases (e.g. Fountain 1986, Kukkonen & Lahtinen 2001).

4.5.2 Tectonic setting

Consistent differences in chemical composition have long been used to discriminate between different tectonic settings (e.g. Pearce & Cann 1973). Since the purpose of this contribution is to characterise the heat production of different geological provinces, there is a certain lumping of different lithologies formed in different tectonic settings. I therefore base this discussion on 3 provinces that display rather narrow lithological variation and the tectonic setting is relatively well defined. The Palaeoproterozoic Transscandinavian Igneous Belt (TIB) consists of granitic rocks formed along the active margin of Baltica in a subduction setting, and yields a median heat production of 2.57 $\mu W/m^3$. The Post-Sveconorwegian granites formed during the Early Neoproterozoic, following the Sveconorwegian orogeny. Although the process(es) leading to their formation is uncertain, it is clear that they formed in an intracontinental setting. The Post-Sveconorwegian granites yield a median heat production of 3.92 $\mu W/m^3$. The Permian Oslo Rift represents magmatic rocks formed in an intracontinental rift and yields a median heat production of 2.50 $\mu W/m^3$. However, the Oslo Rift consists of a variety of rock types including syenites and other intermediate rocks, as well as basalts. Including only Permian granites in the calculation yields a median heat production of 3.23 $\mu W/m^3$. These results compare well with numerous investigations showing that rocks formed in continental, extensional settings, be it continental back-arcs, continental rifts, or post-orogenic extension, are enriched in incompatible elements (Frost et al. 1999, Slagstad et al. 2004, Anderson & Morrison 2005). There are probably a number of reasons for the difference in composition between rocks formed in intraplate and plate margin settings. The most obvious difference is that most plate margin magmas form by partial melting in the mantle wedge overlying a subduction zone, whereas intraplate magmas commonly form in areas where upwelling of hot asthenospheric melts induces partial melting of lower crustal rocks. Lower crustal rocks, although generally depleted relative to upper crustal rocks, are significantly more enriched in heat producing elements than the mantle wedge, thus providing a source for relatively enriched magmas. Tectonic setting can therefore be used as a rough guide to a province's heat production.

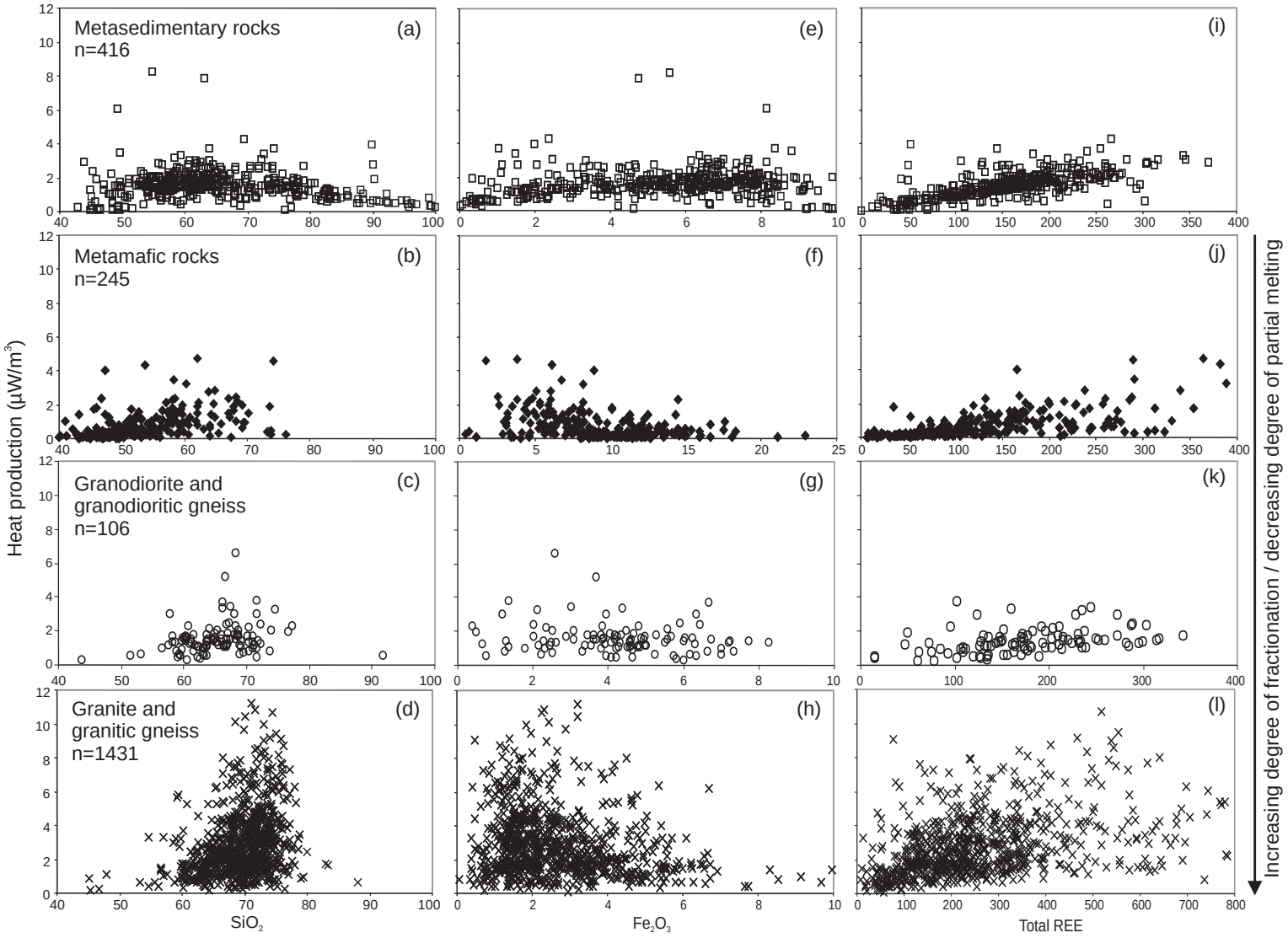

Figure 4.3. Heat production vs. chemical composition sorted by rock type.

4.6 Heat production vs. age and metamorphic grade

4.6.1 Age

Radiogenic heat production is sometimes considered to decrease with increasing age, although some studies fail to find such a correlation (e.g. Kukkonen & Lahtinen 2001). Fig. 4.2 shows the heat production rates of the various geological provinces considered here, broadly arranged in chronological order. Fig. 4.2 shows that there is no clear-cut relationship between geological age and heat production, despite the fact that the Archaean gneisses display relatively low heat production rates, with a median of 0.81 ± 1.48 μW/m^3. This is similar to that of Archaean gneisses in Finland (0.79 ± 1.33 μW/m^3, Kukkonen & Lahtinen 2001). However, both the Palaeoproterozoic Lofoten and the Early Neoproterozoic Egersund AMCG complexes display significantly lower heat production rates. Notably, the two AMCG complexes display similar heat production rates despite an age difference of c. 900 million years. This shows that lithological variation exerts a first-order control on heat production. It is therefore more relevant to compare the Archaean gneisses with younger provinces with a similar lithological make up, in particular the Sveconorwegian province in South Norway and the Western Gneiss Region. These provinces consist mainly of Mesoproterozoic intermediate to felsic gneisses, not unlike the Archaean gneisses, but have heat production rates that are somewhat higher (Table 4.2, Fig. 4.2). The available data indicate that a correlation between heat production and geological age may exist, but that this correlation is weak and in most cases obscured by lithological variation. This conclusion is further supported by data from the Palaeoproterozoic Transscandinavian Igneous Belt and the Permian Oslo Rift, which both consist largely of granitoid rocks and display virtually identical heat production despite an age difference of nearly 1.5 billion years. Thus, predicting heat production rates based on geological age clearly is not feasible, a conclusion which is in line with that proposed by Kukkonen & Lathinen (2001).

4.6.2 Metamorphic grade (crustal depth)

Many workers assume that heat production decreases with increasing metamorphic grade or crustal depth because during orogenesis, partial melting at lower to middle crustal levels commonly form melts rich in incompatible elements, including the heat producing elements, may migrate to higher structural levels (e.g. Slagstad et al. 2005). This leads to a depletion of high producing elements at low crustal levels, and concomitant enrichment at higher crustal levels where the melts are emplaced as plutons (Sandiford & McLaren 2002, Sandiford et al. 2002). Although the concept of a rather homogeneous, low-heat producing lower crust is clearly oversimplified (cf. Flowers et al. 2006), it has long been recognised that the middle and lower crust must be depleted in heat producing elements relative to the upper crust to avoid impossibly high temperatures at depth within the crust (e.g. Morgan & Sass 1984). Unfortunately, true lower crustal rocks are exposed in only a few locations in the world, but several studies investigating the variation in heat production in vertical cross sections through the middle to upper crust have been undertaken. Ashwal et al. (1987) investigated a c. 25 km thick vertical section through amphibolite- to granulite-facies Archaean rocks in the Kapuskasing area, Superior Province, Ontario. Their work showed no relationship between vertical depth/metamorphic grade and heat production, which they suggested could be a

typical feature of rather "mafic" geological provinces, whereas more "granitic" provinces are more likely to display such a relationship. Brady et al. (2006) presented heat production data from the Sierra Nevada Batholith, California, and showed that it increased from c. 2 to 3 $\mu W/m^3$ in the uppermost 5 km, then dropped to 0.5–1 $\mu W/m^3$ at 15 km depth and remained constant at that level to the Moho. These studies show that heat production does not vary continuously or predictably with crustal depth, but that abrupt changes related to lithological variation is the norm.

The Lofoten–Vesterålen area in north Norway, including the Lofoten AMCG complex, is sometimes cited as an example of lower crustal rocks having undergone depletion in incompatible elements due to regional metamorphism (Heier & Adams 1965). However, more recent work suggests that the amphibolite- to granulite-facies transition in this area, interpreted by Heier (1960) to be a gradual metamorphic transition, could be a contact metamorphic effect. It is notable that the Lofoten AMCG complex has a heat production that is nearly identical to the unmetamorphosed Egersund AMCG complex, suggesting that the low heat production of the former is lithologically/tectonically controlled.

The above discussion shows that discussions of the impact of metamorphic grade on heat production are hampered by the strong effect of lithological and chemical variation. This means that not only is comparing lithologically different high- and low-grade rocks useless, even comparing lithologically similar high- and low-grade rocks may be meaningless due to the large variation observed among similar rock types. These complexities imply that meaningful investigations into the distribution of heat producing elements and the controlling processes can only be undertaken in areas where the geological setting is particularly favourable. One such area is the Sognefjorden transect, where Caledonian folding and thrusting has resulted in the exposure of a c. 30 km vertical cross section (Milnes et al. 1997) through Sveconorwegian crust. The cross section includes Sveconorwegian granulites (source?), migmatites (melt transfer zone?) and granites (shallow crustal "deposits" of heat producing elements) (Skår & Pedersen 2003), that may reflect processes related to crustal differentiation. Syn-orogenic granites are also found elsewhere in SW Norway (Slagstad & Marker unpub. data 2006), suggesting that the middle to lower crust underwent relatively widespread melting during Sveconorwegian orogenesis. This evolution would have had a major impact on the distribution of heat producing elements and thus the thermal structure of the Sveconorwegian crust, which in turn may have affected its behaviour during subsequent tectonic activity.

4.7 New heat production data

During the summer and fall of 2007, 350 samples were collected, covering all of Finnmark county and all major rock units (Fig. 4.4). The data from these samples will be available in late 2008, and provide a basis for significantly more detailed interpretation regarding heat production in these areas.

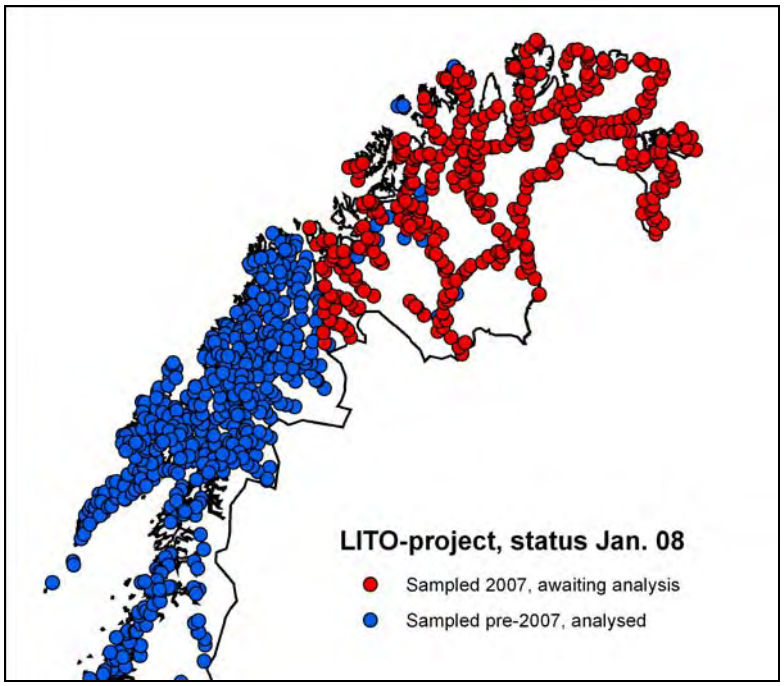

Figure 4.4. Available samples and data from northern Norway.

5 STATUS REPORT GEOCHRONOLOGY

Børre Davidsen, David Roberts and Trond Slagstad, NGU

5.1 Overview

The geochrology work on the offshore basement drill cores, conducted under the HeatBar project forms a continuation of the work conducted under the Kontiki Project.

In total, thirty samples of basement rocks from 22 wells in the North Sea, Norwegian Sea and Barents Sea were obtained from the Norwegian Petroleum Directorate. In the Kontiki Project zircon was separated from 11 samples from the North Sea and Norwegian Sea, and analysed for Pb/U- age determination, either by laser ablation–inductively coupled plasma–mass spectrometry (LA–ICP–MS) at the Geological Survey of Norway and/or by secondary ion mass spectrometry (SIMS) at the Nordsim laboratory in Stockholm. Seven of the samples have been analysed using both techniques.

In this project, six of the remaining offshore drill cores from the Finnmark coast and Barents Sea have been processed for zircon separation. Zircons were retrieved from only three of the samples:

- 7120/12-2, Norwegian Sea: Grey, mylonitic gneiss
- 7128/4-1, Finnmark east, the Barents Sea: Laminated sandstone
- 7128/6-1, Finnmark east, the Barents Sea: Sandstone

while the remaining three were barren:

- 7120/1-1, Loppa High, Norwegian Sea: Orthogneiss/amphibolite
- 7120/2-1, Loppa High, Norwegian Sea: Diabase?
- 7226/11-1, Norsel High, Barents Sea: Biotite schist/gneiss

As there were few offshore data points, and geochronology data sets are absent for parts of the Norwegian mainland, four samples collected by David Roberts from the eastern part of Finnmark were processed as well, as a part of this project. Together with existing data from the western part of Finnmark, these samples will provide the necessary reference frame for the interpretation of the zircon age results from the offshore drill cores.

The results presented below are preliminary, and additional work is required before a final report can be presented.

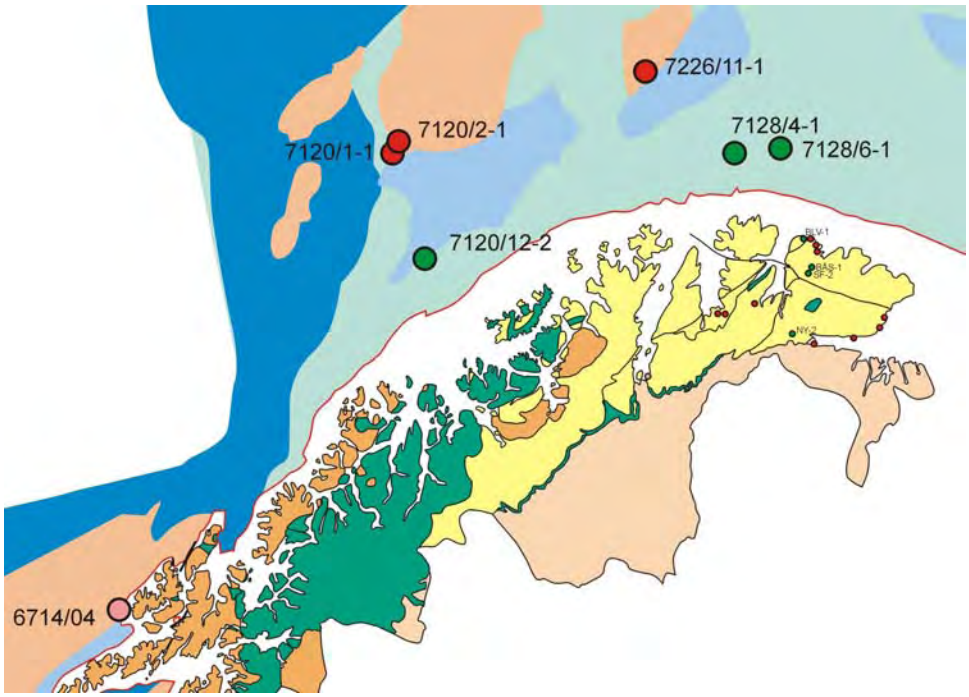

Figure 5.1. Location of the offshore boreholes penetrating cristalline basement. Green dots represent wells for which zircon datings were made.

5.2 Results

Drill core 7120/12-2, from the Norwegian Sea, penetrated a grey, mylonitic gneiss that has been sampled at 4675.8 m depth. Zircons from this sample have been dated to c. 2750-2800 Ma. The protolith most likely presents a felsic intrusive rock, now an orthogneiss. Its composition and age strongly suggests a correlation with the Archaean rocks of Ringvassøya and Vanna in Troms County. Thus, it is probably a NNE-ward continuation of the Precambrian basement present in Lofoten/Vesterålen and on the Troms islands.

The drill cores 7128/4-1 and 7128/6-1, from the Barents Sea, both sampled basement rocks in the form of (unmetamorphosed) sandstones at 2525-2540 m depth. Zircon age dating of sedimentary rocks does not provide an age of emplacement in the same way as with magmatic rocks. Rather, the zircons will display an age spread, reflecting the age of the sources supplying detritus for the sandstone. The youngest zircon in the data set also provides a maximum age for the deposition of the sandstone.

Preliminary results show the same main features for the two samples:
A multimodal spread that extends from c. 1.0 to 1.9 Ga with three groups centred at c. 1.0, around 1.2-1.3 and 1.5-1.8 Ga, with a small subsidiary group at c. 2.6 Ga.

The interpretation of these sandstones will include comparing their ages with those obtained on various sedimentary units on the neighbouring mainland, and constructing a geological history taking into account all relevant factors. This is beyond the scope of this progress report.

In addition, preliminary age determinations have also been obtained on four samples supplied by David Roberts from the Varanger Peninsula:

- NY-2: Nyborg Formation, Tanafjord Group
- BÅS-1 (two samples): Båsnæring Formation, Barents Sea Group.
- SF-2: Sandfjord Formation, Løkvikfjellet Group.
- BLV-1: Berlevåg Formation, Tanahorn Nappe

These samples also represent unmetamorphosed Neoproterozoic sandstones. The results have been presented at EUG in Vienna (by D. Roberts), and the submitted abstract is enclosed in Appendix A.

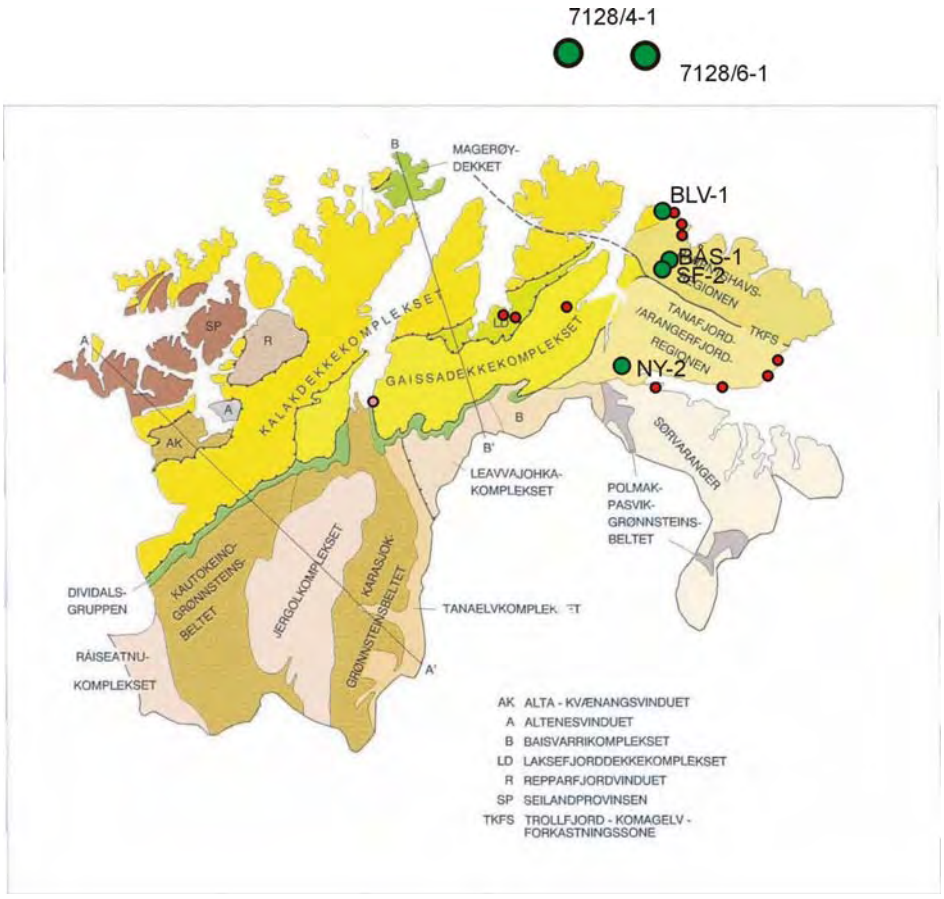

Figure 5.2. Samplig locations onshore Finnmark.

6 GEOPHYSICAL MODELLING

Cécile Barrère, Jörg Ebbing & Laurent Gernigon, NGU

6.1 Introduction

Our study area is the southwestern Barents Sea (69°N–75°N and 13°E – 30°E) which encompasses major structural highs, platforms and lows in the basement (Fig. 6.1) (Faleide et al. 1988, 1991, 1993, Gudlaugsson et al. 1998) facing northern Norway where Caledonian thrusts rest on the Precambrian basement. The Barents Sea shelf reflects a complex history reflected by the basement structure and lithology. The present study aims to investigate the nature of this heritage. Offshore, most of the sedimentary rocks in the basins range in age from Late Palaeozoic to Quaternary. A reliable 3D crustal model of the SW Barents Sea integrating structural information from seismic data and physical rock properties from density and magnetic modelling is in construction. The necessary preliminary work to this 3D modelling was, firstly, the establishment of onshore-offshore links studying potential field data of northern Norway and the western Barents Sea; secondly, the building of 2D regional geological models across the offshore region.

At this stage of the project, the study of the onshore and offshore anomalies combined with geological models result in a basement unit map suggesting the offshore extension of the northern Norway terrains.

6.2 Geology of the western Barents Sea

The basement lithologies and the deformation modes of the Barents Sea area are strongly influenced by Proterozoic and Palaeozoic orogenies. These orogenies are at the origin of the Barents Sea terrains. Literature dealing with the Paleoproterozoic (Karelian) and Neoproterozoic (Timanian) orogenies was studied (Alsgaard 1993, Gee & Tebenkov 2004, Roberts & Olovyanishnikov 2004, Gee et al. 2006, Lorenz et al. 2007).

The most significant tectonic event is the closure of the Iapetus Ocean that involved magmatic activity associated with subduction along the margins of both Laurentia and Baltica from late Cambrian and during a 80 Myrs (Gee 2005). Collision of Baltica with Laurentia began in Silurian times and spanned until early Devonian, resulting in the formation of the Caledonian Mountains. Synchronic magmatism, sedimentation, deformation and metamorphism characterised the early Caledonian evolution to the final collision in early Devonian times. Thereafter, the deformation pattern changed from compression and lateral shortening to regional extension (Gee 2005).

The late Palaeozoic and Mesozoic tectonic history of the Barents Sea was mostly dominated by extensional tectonics. Major rift episodes occurred during Early-Middle Devonian, Carboniferous, Permian, Triassic and Late Jurassic-Early Cretaceous (Johansen et al. 1994). They formed the major rift basins of the Barents Shelf (Fig. 6.1). Continental break-up and

the development of the Barents Margin occurred in mid-Cenozoic (Oligocene) times. The last episode of the complex western Barents Sea history is a regional uplift that started in Cenozoic and led to the removal of several kilometres of sedimentary rocks (Faleide et al. 1996).

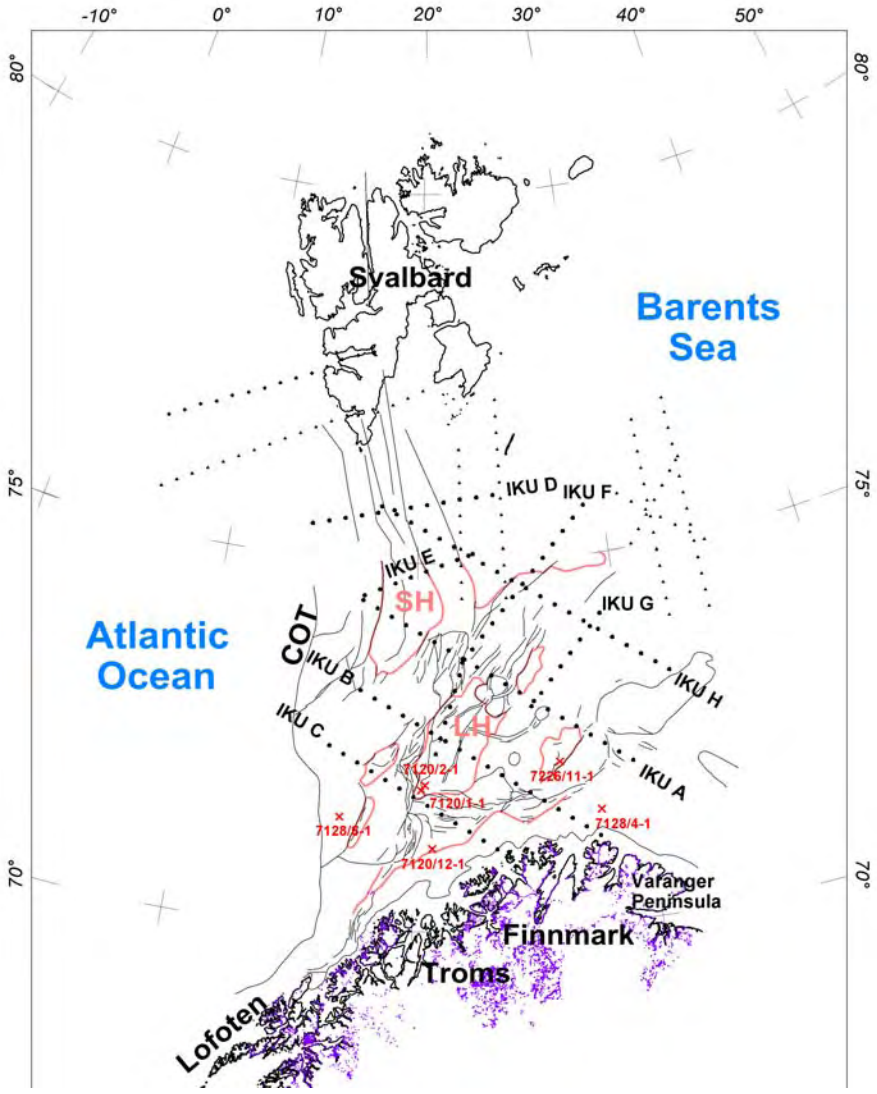

Figure 6.1. ***Simplified structural map of the western Barents Sea. Triangles = refraction seismic profiles (Breivik et al. 2002, 2003, 2005), solid circles = IKU deep seismic reflection profiles, red crosses = exploration wells, purple dots = sample locations for petrophysical measurements.***

6.3 Available data

6.3.1 Seismic data

We had access to depth-converted industrial seismic profiles. The IKU deep seismic reflection lines were particularly studied (Fig. 6.1). Acquired in the mid-1980s, these seismic data have been interpreted in several studies (Gudlaugsson et al. 1987, Faleide et al. 1993, Gudlaugsson

& Faleide 1994, Sanner 1995, Breivik et al. 1998, 2005). We also used the interpretations of intra-basement reflectors carried out by Johansen et al. (1994) and Gudlaugsson et al. (1998). We constrained the boundaries between upper crust and lower crust and the Moho using seismic refraction models (Gabrielsen 1984, Gudlaugsson et al. 1987, Gabrielsen et al. 1990, Gudlaugsson & Faleide 1994, Johansen et al. 1994, Sanner 1995, Breivik et al. 1998, 2002, 2003, 2005, Gudlaugsson et al. 1998).

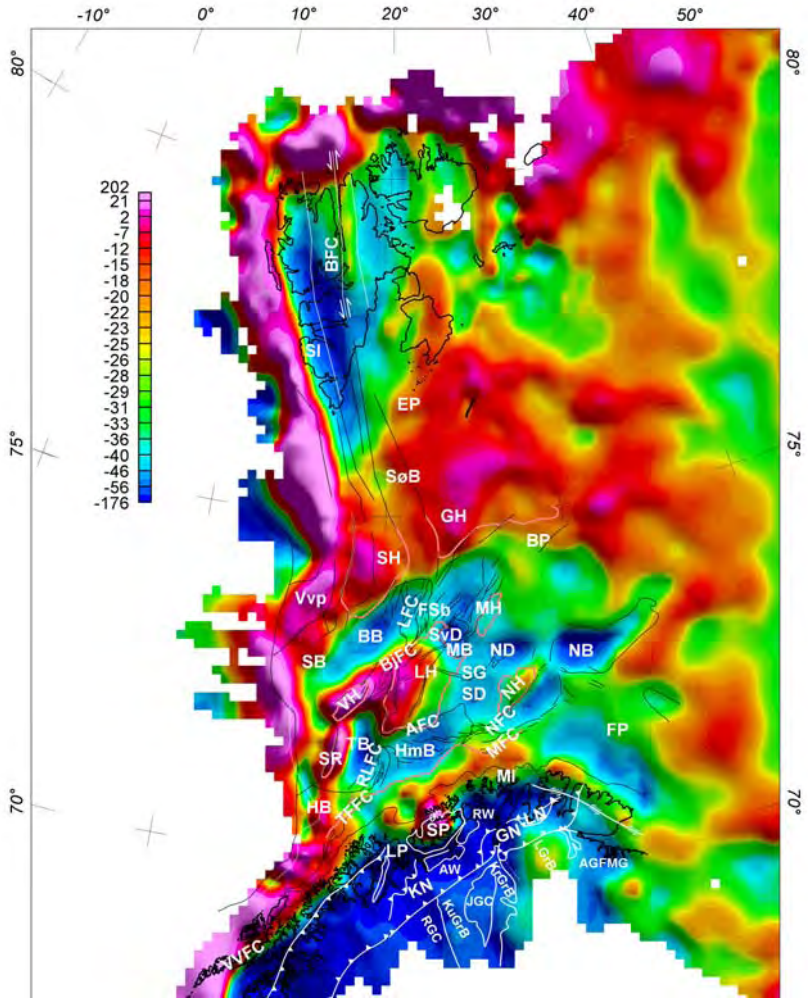

Figure 6.2. Bouguer Anomaly Map (mGal). Bouguer Density = 2.67 kg/m^3.

6.3.2 Gravity data

Gravity data are available from the compilation made by Skilbrei et al. (2000). To make the correlation between the onshore and offshore structures possible, terrain-corrected Bouguer anomaly values were calculated using Bouguer reduction densities of 2670 kg/m^3 (Fig. 6.2).

6.3.3 Magnetic data

Aeromagnetic data are available from the NGU magnetic compilation of the western Barents Sea (Fig. 6.3A). To investigate the deep crustal sources, we reduced the data to the pole and upward continued the magnetic field to 600 m.

Further correlations between tectonic units and magnetic anomalies can be improved by looking at trends from derivative filtered magnetic data. The tilt derivative (Fig. 6.3B) is useful for mapping shallow basement structures. The tilt derivative is defined as the first vertical derivative of the total magnetic intensity, T, divided by the total horizontal derivatives. It enhances the geometrical contrast existing in the internal basement structure (Verduzco et al. 2004).

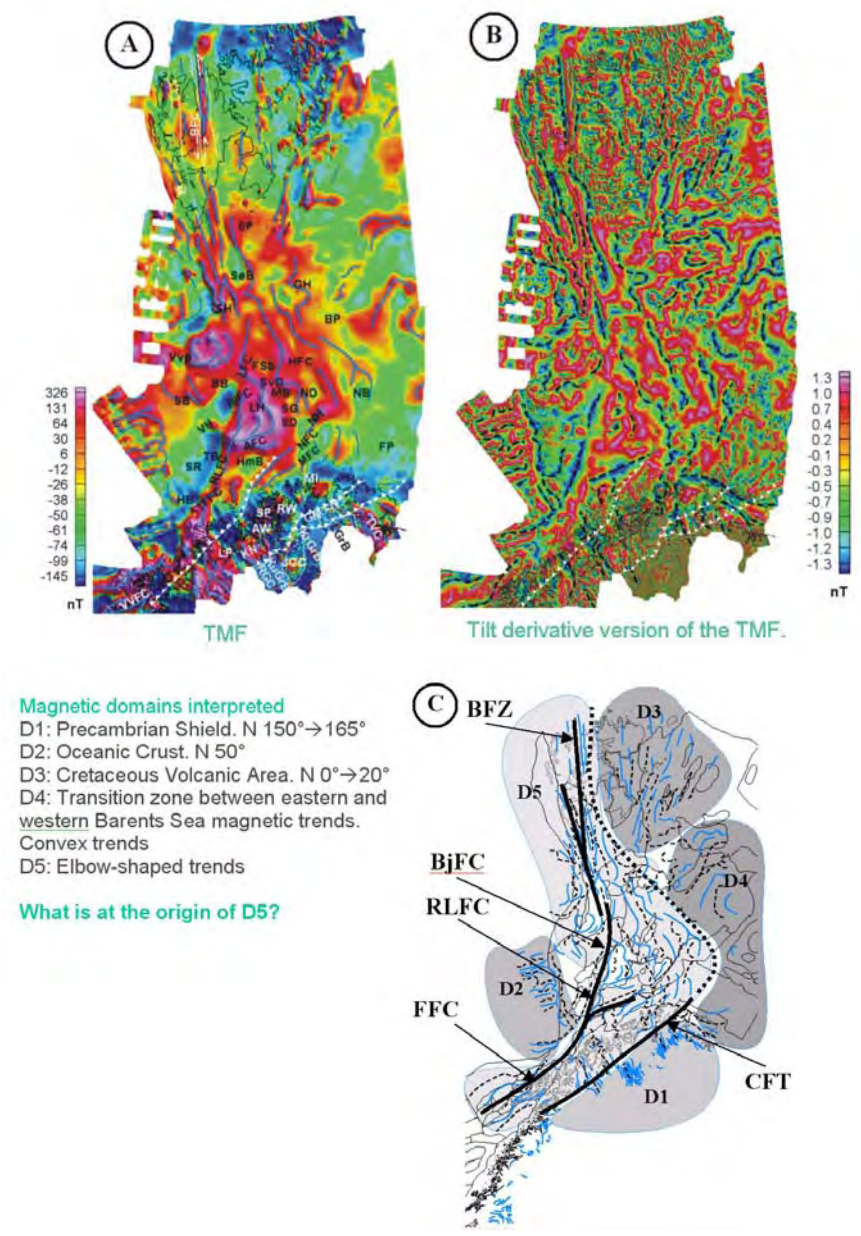

Figure 6.3. (A) Reduced to the pole and upward continued total magnetic field (TMF) and tentative offshore prolongation of main Caledonian thrusts - blue lines represent magnetic trends. (B) Tilt derivative version of the TMF - trends in black dashed lines. (C) Magnetic domains established from the magnetic trends of Fig. 6.3A and 6.3B.

6.3.4 Petrophysical data

Petrophysical data from onshore sampling (Olesen et al. 1990) are used as constraints. Density, magnetic susceptibility and remanence values (Olesen et al. 1990) were considered as starting values for the modelling (Table 6.1).

Table 6.1. Starting values attributed to all geological layers. Densities, magnetic susceptibilities and remanences and Q-ratios adapted from Olesen et al. (1990), Tsikalas (1992) and Breivik et al. (1998, 2002, 2003, 2005). Interpreted values characterise different basement units defined by a combination of petrophysical values obtained by density and magnetic modelling.

Starting values for the modelling				
Unit	Density (kg ·m^{-3})	Mag. susc.	Mag. rem. (A·m^{-1})	Q-ratio
Sedimentary units	1800 to 2710	0	0	0
Precambrian rocks	2750 to 2800	0.01 to >0.1	0.2	0.05 to 0.5
Caledonian nappes	2750	1.10^{-4} to 0.01	0.01	0.25 to 21
Mafic rocks	2800 to 2850	0.01	0.2	0.5
Lower crust	2950	1.10^{-4}	0	0
Mantle	3100 to 3300	0	0	0
Interpreted values				
	Density (kg·m^{-3})	Mag. susc.	Mag. rem. (A·m^{-1})	Q-ratio
B1 Precambrian basement	2750-2800	0.01→0.2	0.2	Q<1
B2 Caledonian basement	2750	0.001→0.01	0.01	Q>1
B3 High density body	3100-3200	0.01→0.2	0.2	Q<0.5
B4 None-magnetic basement	2750-2800	0.0	0	Q=0
B5 Precambrian basement affected by magmatism	2950-2800	0.007	0.2	Q=0.7
MI (Mafic intrusions)	3000	0.015	0.2	0.30→0.35

6.4 Onshore-offshore correlations of gravity and magnetic anomalies

We establish onshore-offshore links correlating the geological information available onshore and offshore with the regional potential fields. We also interpret the maps using different filtering techniques.

6.4.1 Onshore

The outcrops onshore northern Norway reflect the history of the Caledonian orogeny. (Fig. 4A) (Sigmond 1998). The Fennoscandian Shield is partly covered by Caledonian nappes (Fig. 6.2 & 6.4A, B). The Kalak (KN), Gaissa (GN) and Laksfjord (LN) nappes locally reach up to 8 km in thickness (Rice et al. 1989, Olesen et al. 1990, Sigmond 1998). These Caledonian thrust sheets are recognised as major groups of allochtons covering the Fennoscandian

autochthon shield (Roberts & Gee 1985, Lippard & Roberts 1987, Bugge et al. 1995, Gee 2005, Roberts & Lippard 2005). The nappes are locally intruded by mafic rocks whose age is a matter of debate (i.e. Seiland Igneous Province, Magerøy mafic dykes).

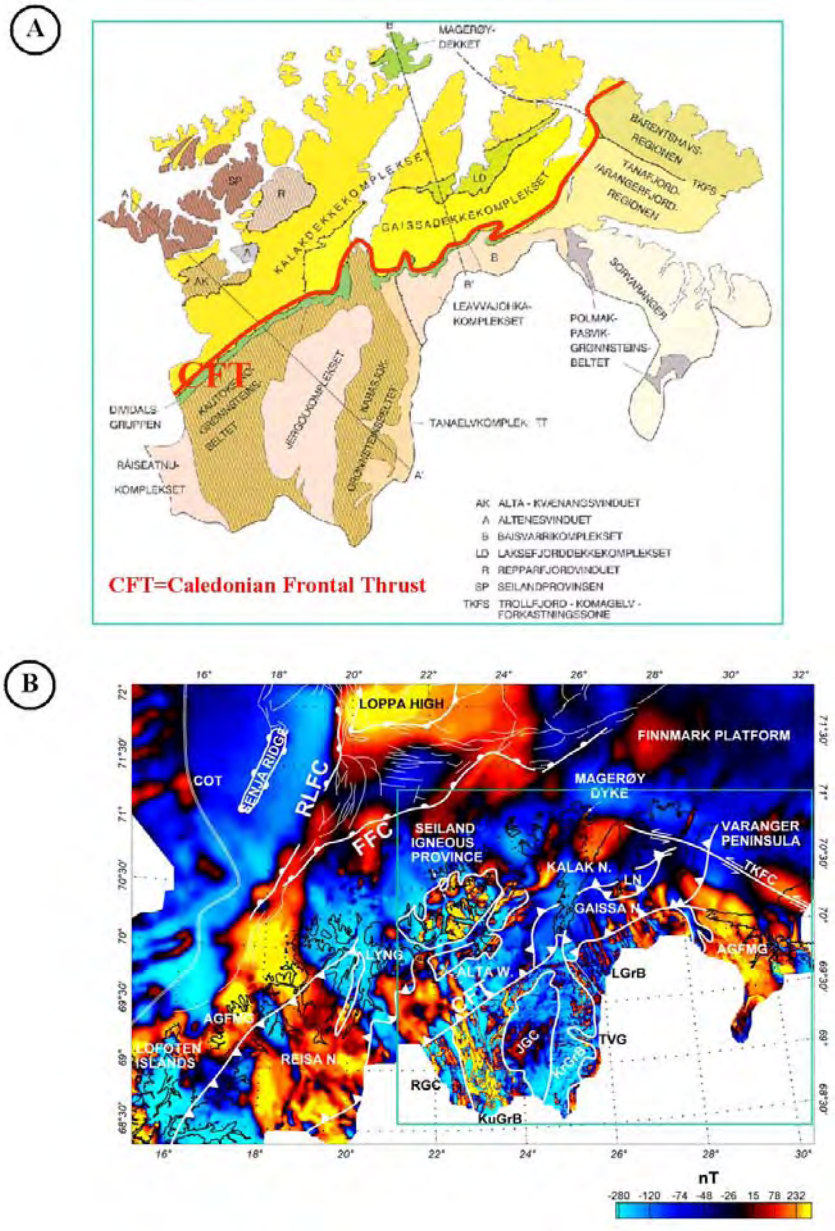

Figure 6.4. (A) Simplified structural map of Finnmark, (B) magnetic anomaly map.

The Bouguer anomaly reflects the density contrast of the anomalous masses with respect to normal densities. The correlation between Bouguer anomalies and onshore geological units is not obvious (Fig. 6.2). The Seiland Igneous Province (SP) creates a pronounced gravity high.

The comparison of the spatial distribution of geological units with the magnetic data (Fig. 6.4B) highlights obvious correlations between Precambrian gneiss complexes and magnetic highs, e.g. the Raisædno (RGC), the Levajok (LGrB) and the Jergol (JGC) gneiss complex (amphibolite facies), the Tanaelv (TVG) migmatite Complex, the Varanger (TVG) Complex

(amphibolite to granulite facies) and the Precambrian granulites facies and migmatitic gneiss N150˚. There is a good correlation between magnetic highs and the mafic complexes (gabbro and ultramafic rocks) of the Seiland magmatic Province as well as with the ophiolites (metagabbros) of the Lyngen Province (LP). The Kautokeino (KuGrB) and the Karajok (KrGrB) greenstone belts (greenshist and amphibolites facies) are associated with a magnetic high but present a distinct lineation striking N165˚ that can be followed underneath the Caledonian nappes (i.e. Kalak Nappe).

Even if the samples from Caledonian nappes are magnetic (Table 6.1.), the thickness of the nappes is insufficient to act as a significant magnetic source. Therefore, Precambrian, mafic and felsic, medium and high-grade metamorphic rocks are recognized as the sources of significant regional magnetic anomalies. These rocks are characterised by different ranges of density and magnetic pattern.

6.4.2 Offshore

Several offshore tectonic units in the study area present a clear gravity signature (Fig. 6.2.). A first-order feature is a prominent ellipsoidal gravity high along and east of the Bjørnøyrenna Fault Complex (BjFC) and the Ringvassøy-Loppa Fault Complex (RLFC). In this area, there is also a magnetic anomaly apparently linked to the basement topography.

The Stappen High (SH), the Veslemøy High (VH) and the Senja Ridge (SJ) are quite well delimited by positive Bouguer anomalies ranging from 30 to 100 mGal. The case of the Loppa High is characterised by a Bouguer anomaly of 70 mGal focused along the Bjørnøyrenna Fault Complex and striking roughly N-S. The Norsel (NH) and the Gardarbanken (GH) highs as well as the Bjarmeland (BP) and the Finnmark (FP) platforms present moderate gravity anomalies from 20 to 30 mGal.

Gravity lows between -20 mGal and -40 mGal outline the Tromsø (TB), Maud (MB), Nordkapp (NB) basins as well as the Norvarg (ND) and Svalis (SvD) salt domes. The Hammerfest (HmB), Bjørnøya (BjFC), Sørvestsnaget (SB) basins and the Samson Dome (SD, salt) correlate with moderate Bouguer anomalies around –10 mGal. The free air (Fig. 2A) and the Bouguer (Fig. 2B) anomalies contain less prominent trends compared to the magnetic data. Nevertheless, the regional N50˚ tectonic trend is visible in lineaments along the Ultrøst Ridge, the Troms-Finnmark (TFFC) and Måsøy (MFC) fault complexes and along the Nordkapp Basin (NB). The gravity highs of the Veslemøy High (VH) and the Senja Ridge (SJ) do not correlate with magnetic highs. In addition, an alignment of gravity highs along the Finnmark Platform mimics a semicircular trend not detectable within the magnetic data.

The upward continued and reduced to the pole total magnetic field (Fig. 6.3A) reflects a combination of top basement topography (i.e. tilted blocks, undulation of erosional surface), intra-basement sources (i.e. high magnetic plutons, mafic dykes) and intra-sedimentary sources (i.e. sills). Therefore, it does not show a good correlation with the offshore tectonic units.

The Loppa (LH) and Stappen (SH) highs, identified as basement highs (Gabrielsen et al. 1990), present strong magnetic anomalies ranging from 100 nT to 900 nT. Some magnetic anomalies are clearly limited in their spatial extension like in the northern part of the Norsel High (NH) and the Veslemøy High (VH). A low-amplitude but well-focused magnetic high is located in the northern part of the Senja Ridge (SJ). The Hammerfest Basin (HmB) is surrounded by several intense magnetic highs. To the north of the basin, the magnetic high is related to the Loppa High (LH). In the southeast, the magnetic high correlates to the junction of three fault complexes: the Tromsø-Finnmark (TFFC), Asterias (AFC) and Nysleppen fault complexes (NFC). To the west, the magnetic high involves the Ringvassøy-Loppa (RLFC) and Tromsø-Finnmark (TFFC) fault complexes. The Svalis (SvD) and Norvarg (ND) salt domes also create positive magnetic anomalies (200 nT). The gravity lows of the Maud Basin (MB) and the faults striking NE-SW in the north of the Maud Basin correlate with high-magnetic anomalies. The Sørvestsnaget Basin (SB) presents a gradual anomaly increasing northwards from -100 to 0 nT. Strong and aligned magnetic lows, in the range of -100 to -160 nT, strike N25˚ and correspond to the Harstad (HB), Tromsø (TB) basins and the eastern part of Bjørnøya Basin (BB).
In the Loppa High (LH) region, two different provinces can be distinguished from potential field data. The western part of the basement high is characterised by a pronounced Bouguer anomaly (70 mGal) and a moderate magnetic one (100 nT). In contrast, the eastern part is marked by a gradual decrease in Bouguer anomalies down to 0 mGal and an increase in magnetic anomalies up to 900 nT.

6.4.3 Identification of magnetic domains

We overlay the trends of the tilt derivative version of the total magnetic field with the trends of the total magnetic field (Fig. 6.3C). Because the magnetic anomaly has a petrophysical and/or structural origin, the magnetic trends outline the pattern of magnetic sources and/or structural elements as contacts between magnetic and less magnetic rocks. Five domains have been identified.

Onshore northern Norway, high frequency magnetic anomalies of the Precambrian gneisses strike N150˚ to N165˚ (Fig. 6.3B, D1). In the southwest, sea floor spreading anomalies strike approximately N50˚; they are bounded by a magnetic high related to the continental/oceanic strike slip system boundary (Fig. 3C, D2). The northeast region around Svalbard was affected by Cretaceous magmatism (Grogan et al. 2000, Maher et al. 2001), on the map it exhibits pronounced and focused linear magnetic anomalies, striking N-S to N20˚ (Fig. 3C, D3). In the east, a group of trends are noticeably different and present a semicircular shape that stops on N150˚ trends by the central part of the area (Fig. 3C, D4).

The central part is defined by north-south trends seen on land in Svalbard. These trends turn N165˚ to N150˚ south of the Svalbard Archipelago and cross the southwestern Barents Sea until the south Loppa High. There, they bend to N50˚ and extend along the Norwegian coast. These trends form an elbow shape and link the N-S trends on Svalbard with the 150˚ trends of the southwestern Barents Sea and the N50˚ trends of the Finnmark, Måsøy and Nysleppen fault complexes (Fig. 3C, D5). The fault zones offshore and parallel to the Lofoten Islands, the Finnmark Fault Complex and the Nordkapp Basin are also aligned N50˚. Onshore, the N50˚ trend corresponds to the strike of the Caledonian thrusts. Therefore, the elbow-shaped magnetic trends offshore are probably the combined effects of the Precambrian pattern and Caledonian thrusts.

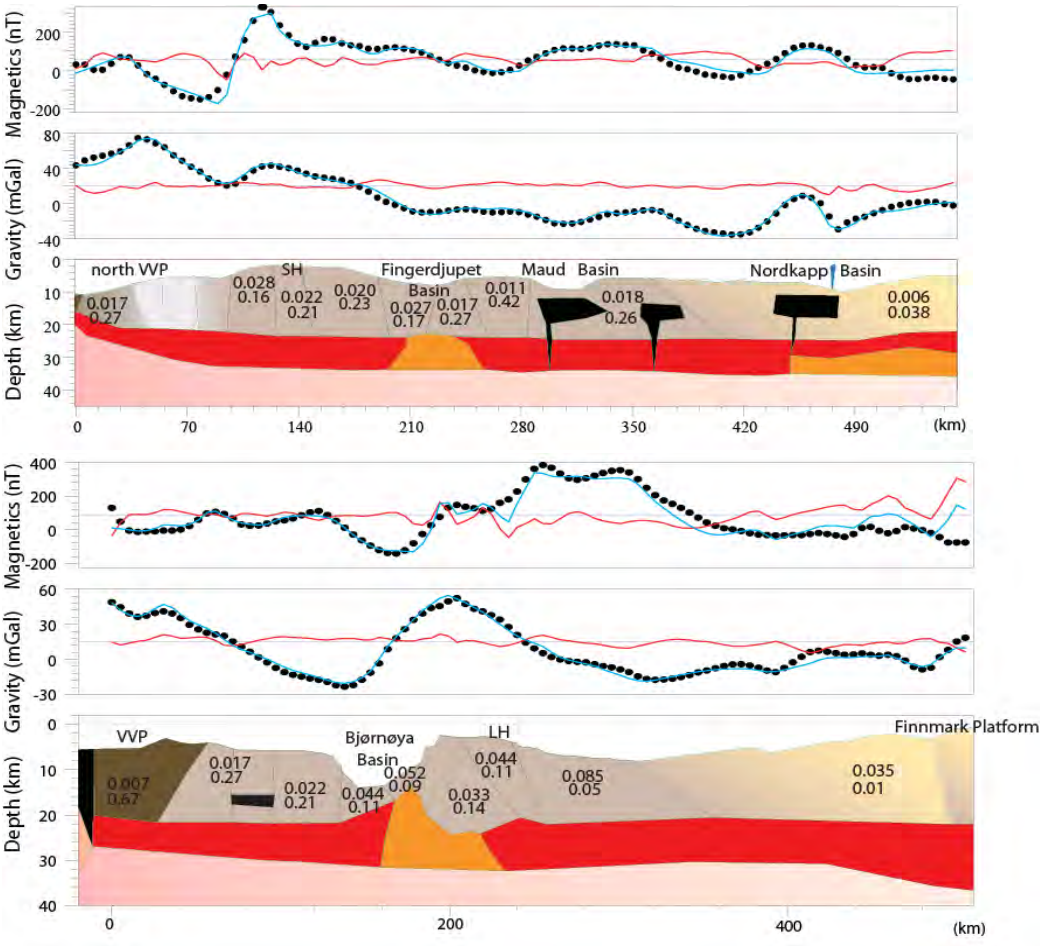

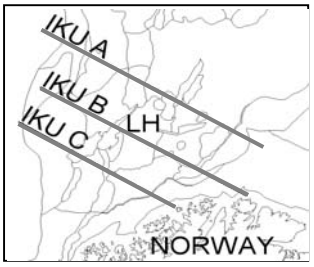

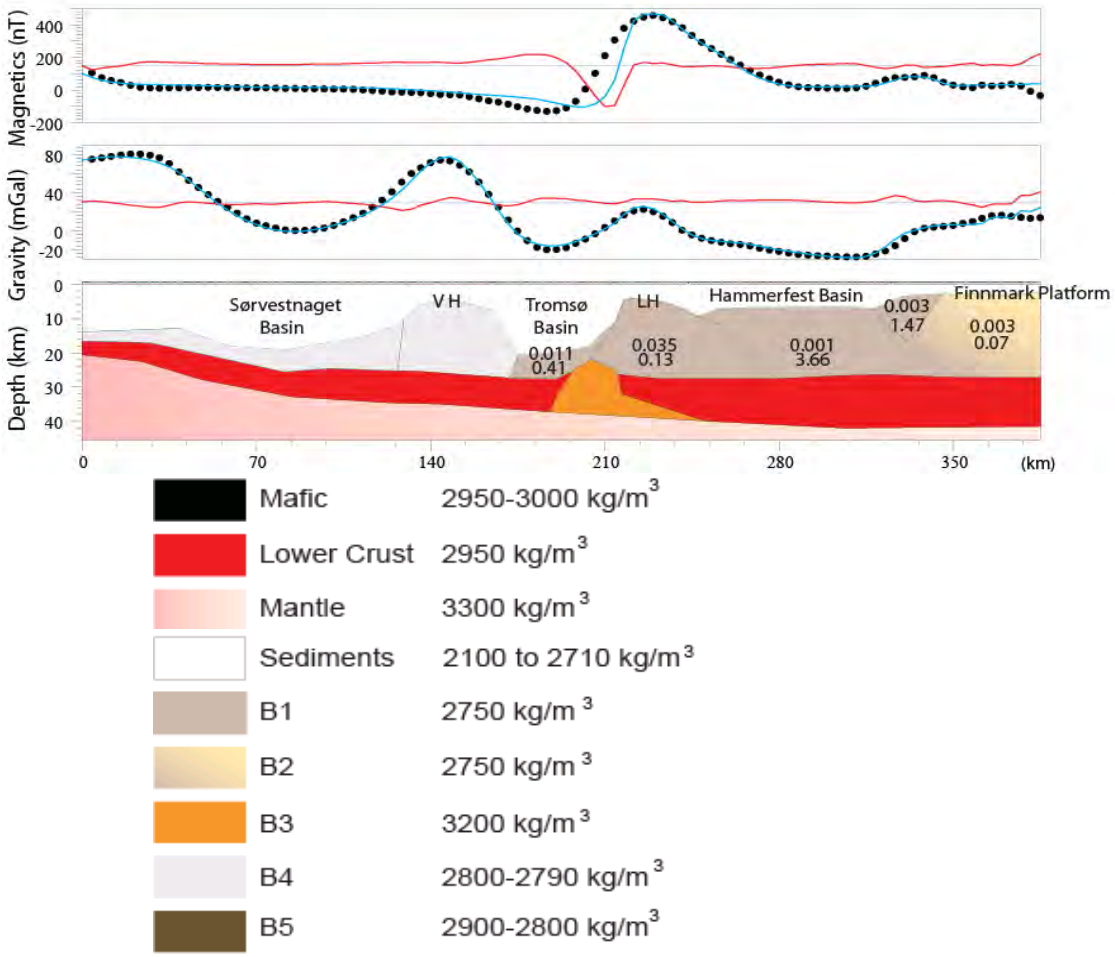

Figure 6.5. Integrated density and magnetic modelling along IKU_A, IKU_B and IKU_C. Numbers represent magnetic susceptibility and Q-ratio values respectively.

6.5 Integrated modelling along IKUA/B/C

The interpretation of the maps is now tested by forward modelling along three NW-SE selected seismic transects IKUA/B/C.

6.5.1 Method

The shallow geometry of the models is based on the interpretation of seismic reflections experiments. Base Quaternary, base Tertiary, intra Upper Cretaceous, intra Lower Cretaceous, base of Upper Jurassic, top Triassic and near top Permian are recognised. The top basement is determined by means of seismic interpretation where possible. Seismic refraction models were used to constrain the deep crustal structure. Another key information derived from the velocity models is the existence of a continuous sub-crustal boundary at 20 km depth where P-wave velocities locally reach 7 km/s; the 20 km depth level is also the depth where basement reflectivity changes (Ritzmann & Faleide 2007) confirming the existence of a boundary between upper crust and middle crust. The reflectivity data along the IKU profiles

published by Ritzmann & Faleide (2007) constrain well the deep lower crust undulation modelled in this study.

After the geometry has been set up, density values were attributed to all layers. The main crustal configuration is based on density modelling. The densities of the sedimentary layers are based on Tsikalas (1992). Tables published by Ritzmann and Faleide (2007) based on velocity-density relationships of sedimentary units obtained from the seismic refraction and reflection/gravity studies are also used (Breivik et al. 1998, 2002, Mjelde et al. 2002, Breivik et al. 2003, 2005) (Table 6.1). In our model we chose a lower crust density of 2950 $kg.m^{-3}$. We start fixing the crustal structure by density modelling. Then, the magnetic modelling splits the crust in blocks of contrasted magnetic properties.

The remanent magnetisation of Precambrian and Caledonian rocks is related to the abundance of magnetic minerals within the rocks, their thermo-mechanical history and the geomagnetic field coeval to formation. Within coarse grain rocks, the inclination and declination are aligned to the present-day geomagnetic field (inclination I=79˚, declination D=4.3˚). The induced magnetisation (H) is proportional to the strength of the induced present-day geomagnetic field (B) (B = 54000.10^{-9} T equivalent H = 42.97 A/m). Aligning the induced magnetization and the remanence magnetization corresponds to adding their respective vectors. Therefore, this simplification tends to give maximum magnetization values and we consider the direction of the remanent field to be the same as for the induced field. The relative importance of remanent magnetisation (Mr) vs. induced magnetisation (Mi) is expressed by the Koenigsberger ratio (Q-ratio).

$$Koenigsberger\_ratio = Q = \frac{|Mr|}{|Mi|} = \frac{Mr}{\chi H} = \frac{remanence}{\chi * 42.97}$$

With χ = susceptibility.

After fixing magnetic remanence and magnetic susceptibility by modelling, this ratio is computed for each block and interpreted considering previously published values. In that region, when magnetic modelling was carried on, only the magnetic susceptibility was taken into account and the magnetic remanence is neglected (Ritzmann & Faleide 2007). Here, in order to compute the Q-ratio magnetic susceptibility and remanence are considered for each unit. In northern Norway, the basement rocks present contrasting grades of metamorphism and, as a consequence, the lithologies and petrophysical parameters are most likely very heterogeneous. From the values published by Olesen et al. (1990) a mean remanence of 0.20 A/m for the Precambrian rocks and mafic complexes and a remanence value of 0.01 A/m for the Caledonian rocks are selected. In detail, the modelling starts with the highest magnetic remanence of 0.20 A/m and the value is reduced to 0.01 A/m if the computed magnetic curve is overestimated. In case the use of 0.01 A/m still overestimates the computed magnetic curve, the remanence is taken equal to 0.00 A/m.

The Curie temperature for magnetite is 580˚C, and therefore we limit the extension of potential magnetic sources to the basement and lower crustal blocks. Sedimentary rocks and rocks below the Moho are assumed to be non-magnetic.

Integrated density and magnetic susceptibility modelling of regional profiles are performed along 2D lines (Fig. 6.5). Then, the profiles are compared and correlated with the potential field maps shown in Fig. 6.2, in order to map basement units at the regional scale (Fig. 6.5). We group blocks of compatible magnetic properties before the interpretation. The geological interpretation is based on three petrophysical properties (Table 6.1): density, magnetic susceptibility and Q-ratio. From our idea, the Q-ratios computed add information regarding the relevancy of the use of the magnetic remanence value. Indeed, we note that for some blocks modelled with 2750 kg/m^3 and a remanence value 0.20 A/m, the computed Q-ratio is more than the maximum or under the minimum Q-ratio value expected for Precambrian basement (Table 6.1). We interpret these inexact estimations of the Q-ratio as an overestimation of the magnetic remanence or an underestimation of the magnetic susceptibility value used in the modelling. Consequently we interpret an indication of a progressive thickening of the Caledonian nappes.

We correlate the geological information available onshore and offshore with the regional potential fields maps. We interpret the maps using different filtering techniques, onshore-offshore links of the aeromagnetic and gravity data.

We started our investigations at the most prominent basement high of the area, the Loppa High (Fig. 6.1), which is surrounded by individual faults or fault complexes that were activated during the formation of this positive basement feature (Gabrielsen et al. 1990).

6.5.2 Modelling results

The A transect is about 550 km long (Figs. 6.1 & 6.5). The IKU_A is the northernmost section in this study. It starts north of the Vestbakken Volcanic Province, crosses the thick crust of the Stappen High (SH), the Leirdjupet Fault Complex to its south, the Fingerdjupet (FSb) and the Maud (MB) basins to the Hoop Fault Complex (HFC). Starting with a maximum gravity high of 75 mGal, the gravity anomaly undulates all along the profile, locally without correlating to the top basement topography. The strong undulation (from –150 to 265 nT) of the magnetic anomaly in the NW becomes smoother between –35 and 135 nT along most of the profile.

Several bodies are modelled within the lower Crust. First of all, as along IKU_C and IKU_B, a deep high-density body of 3200 kg/m^3 is created in the lower Crust (x=225 km, z=30km). In contrast to profiles IKU_C and B, no high reflectivity is observed at the place of the high-density body but instead we can note the absence of reflectivity within a reflective basement and lower crust. Four other high-density bodies are modelled. One is another 3200 kg/m^3 density body in the lower crust necessary to fix the curve to the east of the Nordkapp Basin, the other are three intrusions with a density of 3000 kg/m^3. The easternmost intrusion (density=3000 kg/m^3 and apparent magnetic susceptibility=0.036) is necessary to model the gravity high and associated focused magnetic high at the Norsel High. The two intrusions placed in the deep crust at 305 km and 365 km, density of 3000 kg/m^3 and apparent magnetic susceptibility of 0.047 and of 0.009 respectively, are necessary to model the gravity undulation at the Maud Basin region and the correlated focused magnetic highs.

The basement blocks from 0 to 100 km are modelled with a decreasing density from 2990 to 2750 kg/m^3. All other blocks are modelled with an average crustal density of 2750 kg/m^3. The rather low magnetic susceptibilities (i.e. 0.007 to 0.017) of the first blocks are fixed equal to 0 for the blocks at the east of the Stappen High. From 100 km to 350 km, the blocks have a susceptibility of 0.020 ±0.005. The block from 350 km to the end of the profile is modelled with the low magnetic remanence value of 0.01 A.m^{-1} and a magnetic susceptibility of 0.006.

For the block close to the margin the Q-ratio computation gives 0.60. The adjacent block presents a Q-ratio of 0.27 and the following two blocks are non-magnetic. The block west of Stappen High presents a Q-ratio of 0.9. The blocks from 100 to 280 km present similar Q-ratios of 0.20 ± 0.05. The first intruded block bears a Q-ratio of 0.25 and the two intrusions 0.10 (at 305 km) and 0.39 (at 365 km), respectively. The last block is modelled with a magnetic remanence of 0.01, its Q-ratio is 0.04 and the last intrusion has a Q-ratio of 0.15.

The B transect is 500 km long (Figs. 6.1 & 6.5). The model starts at the vicinity of the margin, crosses the Vestbakken Volcanic Province, then the Bjørnøyrenna Basin, the Loppa High, the north of the Hammerfest Basin and ends on the Finnmark Platform. The profile cuts the middle of the ellipsoidal gravity high at the west of the Loppa High. As for IKU_C, it is necessary to create a high-density body (3200 kg/m^3) in the lower crust to fit the western slope of the gravityanomaly related to the Loppa High. Ritzmann and Faleide (2007) proposed a density model along IKU_B where they put a lower crustal body with a flat top of 2980 kg/m^3 density in a lower crust of 2930 kg/m^3 and upper crust of 2770 kg/m^3. Although our solution differs from that, the shape and the density of the body proposed in our model creates the density contrast able to produce the measured gravity anomaly and both its existence and shape are constrained by the high-reflectivity underneath the Loppa High (Ritzmann & Faleide 2007).

In order to control the edge effect due to the direct contact with the oceanic crust we modelled a block of basalt (density=3000 kg/m^3) as part of the oceanic crust. The adjacent block is part of the volcanic province; its density is high (2800 kg/m^3) and its magnetic susceptibility is 0.007. The rest of the crustal blocks are modelled with the average crustal density 2750 kg/m^3. A small rectangular body with a density 3000 kg/m^3 is added in a block to model a little rebound visible along the gravity curve. At a similar location, horizontal high reflectors were reported by Ritzmann and Faleide (2007). The modelled magnetic susceptibilities increase towards the western flank of the Loppa High from 0.017 to 0.052. The blocks making the highest part of the Loppa High (around 190-230 km) are modelled with a susceptibility of 0.033 and 0.044. The block centred on kilometre 280 and responsible for the two coalescent magnetic anomalies (around 380 nT) is modelled with a magnetic susceptibility of 0.085. The dramatic decrease of the magnetic curve calls for the use of a low remanence value of 0.01 A/m. The blocks are then modelled using a magnetic susceptibility of 0.035.

For the block close to the margin the Q-ratio is 0.67. Modelled with a magnetic remanence of 0.2 A/m, the blocks to the west of the Bjørnøya Basin present a Q-ratio around 0.25; the ones to the east of the Bjørnøya Basin a Q-ratio around 0.15. To the extreme east, the block modelled with a magnetic remanence of 0.01 A/m presents a Q-ratio of 0.01.

The transect C (Figs. 6.1 and 6.5) is 300 km long. The first basement high from the west is the Veslemøy High (VH), the second is the southwestern corner of the Loppa High (LH) and the third is the Finnmark Platform (FP); the basins crossed are the Sørvestsnaget (SB), Tromsø (TB) and Hammerfest (HmB) basins.

The profile cuts the southern extremity of the ellipsoidal gravity anomaly (Fig. 6.2). The two gravity highs at 145 km and 225 km are mostly related to basement highs. The Loppa High block and its well-constrained flanks do not permit a good fit of the western slope of the gravity anomaly. Therefore, a deep high-density body (3200 kg/m^3) is placed in the lower crust (2950 kg/m^3). The northwestern blocks encompass the crust at the vicinity of the margin and the Veslemøy High. They are modelled with a density of 2800 kg/m^3 decreasing to 2790 kg/m^3 towards the Tromsø Basin and their susceptibility is equal to zero. The three neighbouring blocks constitute the Tromsø Basin basement, the Loppa High (LH) and the Hammerfest Basin basement; they are all modelled with an average crustal density of 2750 kg/m^3. The magnetic susceptibility of the basement below the Tromsø Basin is fixed to 0.011 and the ones of the Loppa High and the Hammerfest Basin decrease from 0.035 to 0.001 towards the southeast. The block of the Finnmark Platform is modelled with the average crustal density of 2750 kg/m^3 and its magnetic modelling necessitated the use of a low remanence value (i.e. 0.01 A/m), its susceptibility is then fixed at 0.003. To get the best fit for the magnetic curve and model the magnetic high at the edge of the Finnmark Platform a conic body (density=2750 kg/m^3, magnetic susceptibility=0.003) is added.

For the blocks modelled with a magnetic remanence of 0.20 A/m the Q-ratios are 0.41, 0.13 and 3.66. For the block modelled with a remanence value of 0.01, the Q-ratio is 0.07 and for the conic body modelled with 0.02 A/m, the Q-ratio is 1.47.

6.6 Basement unit map – southwestern Barents Sea

The interpretation of the 2D density and magnetic models allows for discriminating basement lithologies offshore. Onshore-offshore correlations of the lithologies provide a map of the different basement units for the southwestern Barents Sea (Fig. 6.6). The relative distribution of Precambrian and Caledonian rocks is determined by the integrated interpretation of potential field data. The crustal reflectivity previously studied by Ritzmann and Faleide (2007) is included in this new interpretation. Geophysical parameters are shown in Table 6.1.

Five different basement types are distinguished by combining information gained from the models and from the magnetic properties measured on Troms and Finnmark samples. The B1 basement unit is interpreted as being Precambrian in age. At the southeast of the study area, the first B1 unit is the Precambrian Shield cropping out in northern Norway. The second is an onshore-offshore strip starting in the Lofoten Islands, including the outer part of the Troms area and extending towards the NE. The age of 2.8 Ma has been determined from a basement sample from well 7120/12-1 (Fig. 6.1). This dating is described in Chapter 5 and confirms the presence of Precambrian basement right underneath the Palaeozoic sediments at the edge of the Finnmark Platform and, thus, supports our onshore-offshore correlation. A third B1 block

is mapped in the Stappen High region; it includes the Stappen High and northern Sørvestsnaget Basin.

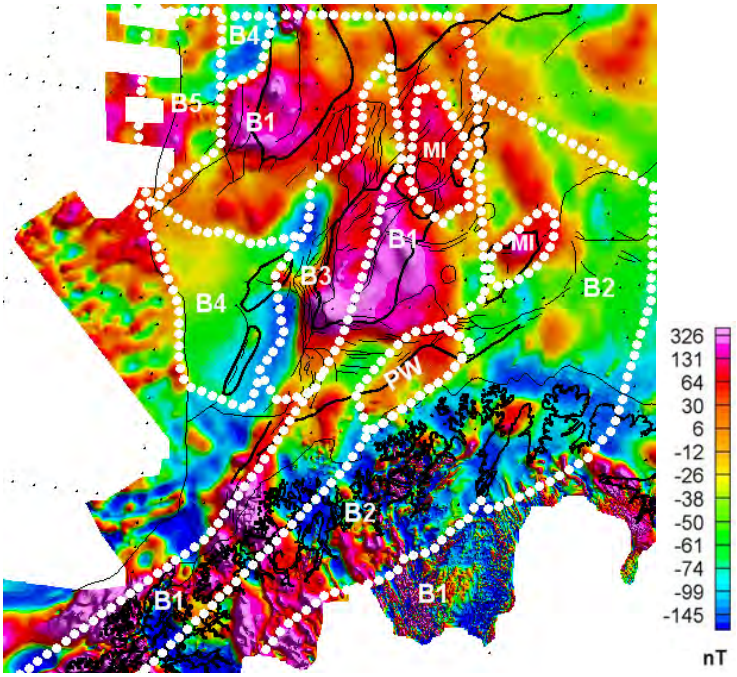

Figure 6.6. Interpreted basement unit map (see text).

The B2 basement unit is interpreted to be Caledonian in age. This implies that the Caledonian nappes are thick enough to hide the signal of the underlying Precambrian basement. Onshore the unit encompasses the Caledonian nappes themselves. Offshore, blocks with a Caledonian signature are modelled at the SE end of profiles IKU_A/B and C.

The B3 unit consists of two high-density bodies recognised in the deep lower crust along profiles IKU_A/B/C. These bodies are interpreted as core-complex bodies. Their density is modelled between 3100 and 3200 kg/m^3 and they may consist of a mixture of low-grade to high-grade metamorphic rocks originating thelower crust and from a possible eclogised former crustal root. These lower crustal bodies of high density are installed directly above the Leirdjupet, Bjørnøya and Ringvassøy-Loppa fault complexes. In our concept the deep and curved reflectors observed to the east of the Ringvassøy-Loppa (RLFC), Bjørnøyrenna (BjFC) and Leirdjupet fault complexes (Ritzmann & Faleide 2007) originate from the emplacement of a core-complex and related mineral modifications. Such a core-complex can develop during post-orogenic collapse. In the study of Ritzmann and Faleide (2007) the high-density lower crustal material at the western margin of the Loppa High has a strong reflectivity and a high velocity (7.2-7.4 km/s) compared to the overlying none-reflective basement and adjacent lower crust. It is not excluded that a fragment of Iapetus oceanic crust related constitutes part of the lower crust.

The units B4 and B5 are distinguished along the margin. In the southwest, B4 extends from the oceanic crust to the high-density lower crust B3. B4 is interpreted as a part of the segmented margin. The absence of correlation between gravity high and magnetic high for the basement highs of Veslemøy High and Senja Ridge could be due to volcanics of inverted polarity going against the polarisation of the basement rocks.

B5 encompasses the Vestbakken Volcanic Province (VVP) and terrains north of it. According to Faleide et al. (1988), the VVP is seismically characterized by a high reflectivity level interpreted as lava flows covering older sedimentary rocks. Some related intrusions are also reported. These volcanics must represent high-density material to to fit the modelled the gravity curve to the observed gravity along the margin. It would be more adequate to place intrusions and lavas flows in the sedimentary layers but a detailed analysis of this area is beyond the scope of the present study.

In addition to the basement units, focused magnetic and gravity anomalies lead to the modelling of two stacks of sills (noted MI in Fig. 6.6 for mafic intrusion) to the north of the Loppa High (IKU_A). Another one is interpreted at the origin of the focused magnetic high characteristic of the Norsel High. Finally, the magnetic highs aligned between the Finnmark Platform and the Hammerfest Basin are interpreted as a Precambrian window (PW) similar to the Alta Window (AW) observed onshore (Fig. 6.4B).

6.7 Ongoing work

6.7.1 Regional Interpretation

The proposed prolongation of basement lithologies towards the north is as yet speculative but insights are possible thanks to the information available on the structure and outcrops of the Svalbard Archipelago, the potential field maps and the seismic lines IKU/D/E/F/H. Indeed the information illustrated by the Figs. 6.3-6.6 will be linked to Svalbard geology and basement reflectivity data along profiles (IKU/D/E/F/H) in the north of the southwestern Barents Sea. A more regional interpretation will be proposed and compared to the present model of the Caledonide extension published so far.

6.7.2 3D Potential Field Model

A 3D model of the southwestern Barents Sea is currently under development using the IGMAS software. IGMAS is an interactive tool of combined density and magnetic 3D modelling. The 3D model is devoted to test our basement units map and will provide a new top basement map, a new Moho map and a 3D geometry for the core-complexes interpreted along the fault complexes to the west of the Loppa High.

7 CONCLUSIONS

7.1 Current status (September 2008)

The HeatBar Project aims at characterising the amount of heat transferred from the underlying basement to the sedimentary basins of the western Barents Sea. This goal will be reached by estimating surface heat flow onshore and offshore and characterizing the U, Th and K content of basement rocks in northern Norway. Geophysical information such as seismic, aeromagnetic, and gravity data will provide a basis for extending this information below the offshore sedimentary basins

Since the start of the HeatBar Project by autumn 2005 the following tasks have been completed:

- ✓ logging for temperature measurements two boreholes (6 visited so far) in Finnmark, thermal conductivities have also been measured in the lab.;
- ✓ drilling down to 720 m of a new borehole by the Vuoddašjav'ri lake in central Finnmark;
- ✓ two heat flow calculations from Båtsfjordfjellet (25 mW/m^2) and Bjørnevatn (preferred value: 66 mW/m^2);
- ✓ 350 samples collected from basement rocks in Finnmark for geochemical analyses (mainly content of heat generating elements);
- ✓ preliminary dating of zircons from basement samples collected offshore in oil exploration wells;
- ✓ establishment, by means of geophysical modelling, of a basement unit map of the western Barents Sea (C. Barrere's PhD thesis, to be defended early 2009);

7.2 Remaining work (until September 2009)

Our remaining tasks for the coming months are:

- ➢ to establish a 3D crustal model of the western Barents Sea (done by Oct. 08);
- ➢ to complete the datings on zircons from offshore/onshore samples (Dec. 08);
- ➢ to correct from paleoclimatic, topographic and structural effects the obtained heat flow values at Båtsfjordfjellet and Bjørnevatn (Oct.-Nov. 08);
- ➢ to calculate heat generation rates from the basement samples collected in Finnmark (Nov.-Dec. 08);
- ➢ to log the cores the Vuoddašjav'ri drillhole and measure thermal conductivity at relevant depths form the hole (Dec. 2008-Feb. 09);
- ➢ to calculate heat production in the wells from ICP-MS data (Jan. 09);
- ➢ to estimate heat flow values offshore from available BHT and DST data (March-Apr. 09);
- ➢ to estimate heat flow from temperature data from the Sysselmannbreen 1000 m deep borehole in Svalbard (Apr. 09);
- ➢ to log the Vuoddašjav'ri well and calculate heat flow (May-Jun. 2009);
- ➢ to build a 3D thermal model for the western Barents Sea (Jan.-Jul. 2009).

The final report of the HeatBar Project will be published by September 2009.

8 REFERENCES

Alsgaard, P. 1993: Eastern Barents Sea late Palaeozoic setting and potential source rocks. *In*: Vorren, T.O. et al. (eds.) *Arctic Geology and Petroleum Potential*. Norwegian Petroleum Society, 405-418.

Anderson, J.L. & Morrison, J. 2005: Ilmenite, magnetite, and peraluminous Mesoproterozoic anorogenic granites of Laurentia and Baltica. *Lithos 80*, 45-60.

Ashwal, L.D., Morgan, P., Kelley, S.A. & Percival, J.A. 1987: Heat production in an Archean crustal profile and implications for heat flow and mobilization of heat-producing elements. *Earth and Planetary Science Letters 85*, 439-450.

Bea, F. 1996: Residence of REE, Y, Th, and U in granites and crustal protoliths: Implications for the chemistry of crustal melts. *Journal of Petrology 37*, 521-552.

Beardsmore, G.R. & Cull, J.P. 2001: *Crustal Heat Flow, a guide to measurement and modelling*, Cambridge University Press, 324 pp.

Brady, R. J., Ducea, M.N., Kidder, S.B. & Saleeby, J.B. 2006: The distribution of radiogenic heat production as a function of depth in the Sierra Nevada Batholith, California. *Lithos, 86*, 229-244.

Breivik, A.J., Faleide, J.I. & Gudlaugsson, S.T. 1998: Southwestern Barents Sea margin: late Mesozoic sedimentary basins and crustal extension. *Tectonophysics, 293*, 21-44.

Breivik, A.J., Mjelde, R., Grogan, P., Shimamura, H., Murai, Y., Nishimura, Y. & Kuwano, A. 2002: A possible Caledonide arm through the Barents Sea imaged by OBS data. *Tectonophysics, 355*, 67-97.

Breivik, A.J. Mjelde, R., Grogan, P., Shimamura, H., Murai, Y. & Nishimura, Y. 2003: Crustal structure and transform margin development south of Svalbard based on ocean bottom seismometer data. *Tectonophysics, 369*, 37-70.

Breivik, A.J. Mjelde, R., Grogan, P., Shimamura, H., Murai, Y. & Nishimura, Y. 2005: Caledonide development offshore-onshore Svalbard based on ocean bottom seismometer, conventional seismic, and potential field data. *Tectonophysics, 401*, 79-117.

Brigaud, F. & Vasseur, G. 1989: Mineralogy, porosity and fluid control on thermal conductivity of sedimentary rocks. *Geophysical Journal, 98*, 525-542.

Bugge, T., Mangerud, G., Elvebakk, G., Mørk, A., Nilsson, I., Fanavoll, S. & Vigran, J.O. 1995: The upper Palaeozoic succession on the Finnmark Platform, Barents Sea. *Norsk Geologisk Tidsskrift, 7*, 3-30.

Bullard, E.C. 1939: Heat flow in South Africa, *Proceedings of the Royal Society of London A, 173*, 474-503.

Carslaw, H.S. & Jaeger, J.C. 1959: *Conduction of heat in solids*, London, Oxford University Press, 386 pp.

Corfu, F. 2004: U-Pb age, setting and tectonic significance of the anorthosite-mangerite-charnockite suite, Lofoten-Vesterålen, Norway. *Journal of Petrology 45*, 1799-1819.

Faleide, J.I., Myhre, A.M. & Eldholm, O. 1988: Early Tertiary Volcanism at the western Barents Sea margin. *In*: Morton A.C. and Parson L.M. (eds.), *Tertiary Volcanism and the Opening of the NE Atlantic*. Geological Society Special Publication, 135-146.

Faleide, J.I., Gudlaugsson, S.T., Eldholm, O., Myhre, A.M. & Jackson H.R., 1991: Deep Seismic Transects across the Sheared Western Barents Sea-Svalbard Continental-Margin. *Tectonophysics, 189*, 73-89.

Faleide, J.I., Vagnes, E. & Gudlaugsson, S.T. 1993: Late Mesozoic-Cenozoic Evolution of the South-Western Barents Sea in a Regional Rift Shear Tectonic Setting. *Marine and Petroleum Geology, 10*, 186-214.

Faleide, J.I., Solheim, A., Fiedler, A., Hjelstuen, B.O., Andersen, E.S. & Vanneste, K 1996: Late Cenozoic evolution of the western Barents Sea-Svalbard continental margin. *Global and Planetary Change, 12,* 53-74.

Flem, B., Grimstvedt, A., Slagstad, T. & Skår, Ø. 2005: Bulkanalyse av Th og U i bergartsprøver med LA-ICP-MS. Metodebeskrivelse.

Flowers, R.M., Mahan, K.H., Bowring, S.A., Williams, M.L., Pringle, M.S. & Hodges, K.V. 2006: Multistage exhumation and juxtaposition of lower continental crust in the western Canadian Shield: Linking high-resolution U-Pb and $^{40}Ar/^{39}Ar$ thermochronometry with pressure-temperature-deformation paths. *Tectonics 25*, doi:10.1029/2005TC001912.

Fountain, D.M. 1986: Is there a relationship between seismic velocity and heat production for crustal rocks? *Earth and Planetary Science Letters 79*, 145-150.

Frost, C.D., Frost, B.R., Chamberlain, K.R. & Edwards, B.R. 1999: Petrogenesis of the 1.43 Ga Sherman batholith, SE Wyoming, USA: A reduced, rapakivi-type anorogenic granite. *Journal of Petrology 40*, 1771-1802.

Gabrielsen, R.H. 1984: Long-lived fault zones and their influence on the tectonic development of the southwestern Barents Sea. *Journal of the Geological Society, 141,* 651-662.

Gabrielsen, R.H., Færseth, R.B., Jensen, L.N., Kalheim, J.E. & Riis, F. 1990: Structural elements of the Norwegian continental shelf. Part I: The Barents Sea Region. *Norwegian Petroleum Directorate Bulletin, 6,* 33.

Gee, D.G. 2005: Scandinavian Caledonides (with Greenland). *In*: Selley R.C., Cocks L.R.M. and Plimer I.R. (eds). *Encyclopedia of Geology*, pp. 64-74.

Gee, D.G. & Tebenkov, A. 2004: Svalbard: a fragment of the Laurentian margin. *In*: Gee D.G. & Pease V.L. (eds.), *The Neoproterozoic Timanide Orogen of eastern Baltica: introduction*. Geological Society London, 191-206.

Gee, D.G., Bogolepova, O.K. & Lorenz, H. 2006: The Timanide, Caledonide and Uralide orogens in the Eurasian high Arctic, and relationships to the palaeo-continents Laurentia, Baltica and Siberia. *In*: Gee D.G. and Stephenson R.A. (eds.), *European Lithosphere Dynamics*. Geological Society of London, 507-521.

Grogan, P., Nyberg, K., Fotland, B., Myklebust, R., Dahlgren, S. & Riis, F. 2000: Cretaceous magmatism south and east of Svalbard: evidence from seismic reflection and magmatic data. *Polar Research, 68,* 11-13.

Gudlaugsson, S.T. & Faleide, J.I. 1994: The continental margin between Spitsbergen and Bjørnøya. *In*: Eiken O. (ed.), *Seismic Atlas of Western Svalbard*, Medd. Norwegian Polarinstitut, 11-13.

Gudlaugsson, S.T., Faleide, J.I., Fanavoll, S. & Johansen, B. 1987: Deep Seismic-Reflection Profiles across the Western Barents Sea. *Geophysical Journal of the Royal Astronomical Society, 89,* 273-278.

Gudlaugsson, S.T., Faleide, J.I., Johansen, S.E. & Breivik, A.J. 1998: Late Palaeozoic structural development of the South-western Barents Sea. *Marine and Petroleum Geology, 15,* 73-102.

Johansen, S.E., Henningsen, T., Rundhovde, E., Sæther, B.M., Fichler, C. & Rueslatten, H.G. 1994: Continuation of the Caledonides North of Norway - Seismic Reflectors within the Basement beneath the Southern Barents Sea. *Marine and Petroleum Geology, 11,* 190-201.

Lippard, S.J. & Roberts, D. 1987: Fault systems in Caledonian Finnmark and the southern Barents Sea. *Norsk Geologisk Tidsskrift, 410,* 55-64.

Lorenz, H., Gee, D.G. & Whitehouse, M.J. 2007: New geochronological data on Palaeozoic igneous activity and deformation in the Severnaya Zemlya Archipelago, Russia, and

implications for the development of the Eurasian Arctic margin. *Geological Magazine, 144*, 105-125.

Heier, K.S. 1960: Petrology and chemistry of high-grade metamorphic and igneous rocks on Langøy, Northern Norway. *Norges geologiske undersøkelse 207*, 1-246.

Heier, K.S. & Adams, J.A.S. 1965: Concentration of radioactive elements in deep crustal material. *Geochimica et Cosmochimica Acta 29*, 53-61.

Killeen, P.G. & Heier, K.S. 1975: Radioelement distribution and heat production in Precambrian granitic rocks, southern Norway. *Det Norske Videskaps-Akademi, I. Mat.-Naturv. Klasse. Skrifter, Ny Serie 35*, 1-32.

Kukkonen, I.T. & Lahtinen, R. 2001: Variation of radiogenic heat production rate in 2.8-1.8 Ga old rocks in the central Fennoscandian shield. *Physics of the Earth and Planetary Interiors 126*, 279-294.

Maher, H.D., Bergh, S., Braathen, A., Manby, G. & Lyberis, N. 2001: Discussion on pre-ocean opening compression of the Northwestern Atlantic margin: evidence from eastern Greenland - Journal, Vol. 157, 2000, 707-710. *Journal of the Geological Society, 158,* 728-730.

McLaren, S., Sandiford, M., Neumann, N., Wyborn, L. & Bastrakova, I. 2003: The hot southern continent: Heat flow and heat production in Australian Proterozoic terranes *Geological Society of Australia Special Publication*. 22, 151-161.

Middleton, M. 1993: A transient method of measuring the thermal properties of rocks. *Geophysics 58*, 357-365.

Milnes, A.G., Wennberg, O.P., Skår, Ø. & Koestler, A.G. 1997: Contraction, extension and timing in the South Norwegian Caledonides: The Sognefjord transect. *In:* Burg, J.-P. & M. Ford (eds.) *Orogeny Through Time*. Geological Society Special Publication 121, 123-148.

Mjelde, R., Breivik, A.J., Elstad, H., Ryseth, A.E., Skilbrei, J.R., Opsal, J.G., Shimamura, H., Murai, Y. & Nishimura, Y. 2002: Geological development of the Sorvestsnaget Basin, SW Barents Sea, from ocean bottom seismic, surface seismic and gravity data. *Norwegian Journal of Geology, 82,* 183-202.

Morgan, P. & Sass, J.H. 1984: Thermal regime of the continental lithosphere. *Journal of Geodynamics 1*, 143-166.

Olesen, O., Roberts, D., Henkel, H., Lile, B.L. & Torsvik, T.H. 1990: Aeromagnetic and gravimetric interpretation of regional structural features in the Caledonides of West Finnmark and North Troms, northern Norway. *Norsk Geologisk Tidsskrift, 419,* 1-24.

Olesen, O., et al. 2007: *Kontiki Final Report, Continental Crust and Heat Generation in 3D.* NGU Report 2007.042 (confidential), 438 pp.

Ormaasen, D.E. 1976: Geochemistry and petrology of the mangeritic rocks in Lofoten-Vesterålen Cand. real./M.Sc. thesis, University of Oslo.

Pearce, J.A. & Cann, J.R. 1973: Tectonic setting of basic volcanic rocks determined using trace element analyses. *Earth and Planetary Science Letters 19*, 290-300.

Raade, G. 1973: Distribution of radioactive elements in the plutonic rocks of the Oslo region [Hovedoppgave/M.Sc. thesis], Universitetet i Oslo, 162 pp.

Rice, A.H.N., Gayer, R.A., Robinson, D. & Bevins, R.E. 1989: Strike-Slip Restoration of the Barents Sea Caledonides Terrane, Finnmark, North Norway. *Tectonics, 8,* 247-264.

Ritter, U., Zielinski, G.R., Weiss, H.M., Zielinski, R.L.B., & Sættem, J. 2004: Heat flow in the Vøring Basin, Mid-Norwegian Shelf. *Petroleum Geoscience 10*, 353-365.

Ritzmann, O. & Faleide, J.I. 2007: The Caledonian basement of the western Barents Sea. *Tectonics, 26,* doi:10.1029/2006TC002059.

Roberts, D. & Gee, D.G. 1985: An introduction to the structure of the Scandinavian Caledonides. *In*: Gee D.G. & Sturt B.A. (eds.), *The caledonian orogen: Scandinavia and Related Areas*. J. Wiley, Chichester, pp. 55-68.

Roberts, D. & Olovyanishnikov, V. 2004: Structural and tectonic development of the Timanide orogen. *Geological Society London Memoirs, 30,* 47-57.

Roberts, D. & Lippard, S.J. 2005: Inferred Mesozoic faulting in Finnmark: current status and offshore links. *Norges Geologiske Undersøkelse Bulletin, 443,* 55-60

Rybach, L. 1988: Determination of heat production rate. *In* Hänel, R., L. Rybach & L. Stegena (eds.) *Handbook of Terrestrial Heat-Flow Determination*. Dordrecht, Kluwer Academic Publishers, 125-142.

Sandiford, M. & McLaren, S. 2002: Tectonic feedback and the ordering of heat producing elements within the continental lithosphere. *Earth and Planetary Science Letters 204,* 133-150.

Sandiford, M., McLaren, S. & Neumann, N. 2002: Long-term thermal consequences of the redistribution of heat-producing elements associated with large-scale granitic complexes. *Journal of Metamorphic Geology 20,* 87-98.

Sanner, S. 1995: Et seismisk hastighetsstudium i Barentshavet Cand. real./M.Sc. thesis, University of Oslo.

Sigmond, E.M.O. 1998: Geologisk kart over Norge. Berggrunnsgeologisk kart ODDA, M 1: 250 000. *Norges geologiske undersøkelse, Trondheim.*

Skilbrei, J.R., Kihle, O., Olesen, O., Gellein, J., Sindre, A., Solheim, D. & Nyland, B. 2000: Gravity anomaly map Norway and adjacent ocean areas, scale 1:3 Million. Geological Survey of Norway, Trondheim.

Skår, Ø. & Pedersen, R.B. 2003: Relations between granitoid magmatism and migmatization: U-Pb geochronological evidence from the Western Gneiss Complex, Norway. *Journal of the Geological Society of London 160,* 935-946.

Slagstad, T., Culshaw, N.G., Jamieson, R.A. & Ketchum, J.W.F. 2004: Early Mesoproterozoic tectonic history of the southwestern Grenville Province, Ontario: Constraints from geochemistry and geochronology of high-grade gneisses. In: Tollo, R. P., L. Corriveau, J. McLelland & M. J. Bartholomew eds. *Proterozoic tectonic evolution of the Grenville orogen in North America*. Geological Society of America, Memoir 197, 209-241.

Slagstad, T., Jamieson, R.A. & Culshaw, N.G. 2005: Formation, crystallisation, and migration of melt in the mid-orogenic crust: Muskoka domain migmatites, Grenville Province, Ontario. *Journal of Petrology 46,* 893-919.

Tsikalas, F. 1992: *A study of seismic velocity, density and porosity in Barents Sea wells (N. Noway)* [Hovedoppgave/M.Sc. thesis], Universitetet i Oslo.

Verduzco, B., Fairhead, J.D., Green, C.M. & MacKenzie, C. 2004: New Insights into MagneticDerivatives for Structural Mapping. *The Leading Edge, 23,* 116-119.

9 APPENDIX A

Detrital zircon age record of platformal and basinal Neoproterozoic sandstones from Varanger Peninsula, North Norway: a preliminary study

D. Roberts, B. Davidsen and T. Slagstad
Geological Survey of Norway, 7491 Trondheim, Norway.

Neoproterozoic to Cambrian sedimentary assemblages on Varanger Peninsula, northern Norway, are separated into platformal and basinal domains along the NW-SE-trending, Trollfjorden-Komagelva Fault Zone (TKFZ). Platformal successions southwest of the fault range from autochthonous to allochthonous and comprise the fluvial to shallow-marine Vadsø, Tanafjord and Vestertana groups. Northeast of the fault zone, successions are allochthonous and most have been involved in modest dextral strike-slip translation along the fault. They comprise the Barents Sea Group, the unconformably overlying Løkvikfjellet Group, and slightly higher-grade rocks of the Tanahorn Nappe.

In an ongoing detrital zircon provenance study of several formations from Varanger Peninsula and adjacent areas, we have carried out LA-ICP-MS, U-Pb analyses on five samples from four representative sandstone units. One formation, the inter-tillite, Vendian, Nyborg Formation, is from south of the TKFZ, and two (Båsnæring and Sandfjord formations) from north of the fault. The fourth sandstone unit analysed is from the Berlevåg Formation in the Tanahorn Nappe. Preliminary results obtained from these formations show the following main features of the detrital zircon populations:

1. *Nyborg Formation, Tanafjord Group (sample NY2)*: one group dominates the probability plot at 2.0-1.7 Ga with a minor spread of mostly discordant grains between 3.0 and 2.5 Ga.
2. *Båsnæring Formation, Barents Sea Group (BÅS1; two samples)*: a multimodal spread extends from c. 2.1 to 1.0 Ga with three peaks of concordant grains at around 1.80-1.65, 1.45-1.40 and 1.2-1.0 Ga, and subsidiary peaks at c. 2.0 and 2.9-2.6 Ga.
3. *Sandfjord Formation, Løkvikfjellet Group (SF2)*: two principal groups at 2.0-1.7 and 2.9-2.6 Ga with a subsidiary group ranging from 1.6 to c. 1.0 Ga.
4. *Berlevåg Formation, Tanahorn Nappe (BLV1)*: one major group at 1.9-1.7 Ga and a minor group at 2.9-2.6 Ga.

A feature common to all these analyses is the presence of a detrital population peak at c. 2.0-1.7 and a subsidiary peak at 2.9-2.6 Ga. From the known stratigraphical and sedimentological picture, with palaeocurrent data indicating that detritus in both the pericratonic and basinal (submarine fan and deltaic) domains came largely from southerly source regions, this is consistent with derivation from the Fennoscandian Shield. Northern parts of this craton are dominated by Neoarchaean complexes and, just to the south, also by terranes of Palaeoproterozoic age deformed during the 1.9-1.8 Ga Svecofennian orogeny. The fact that even the Berlevåg Formation (in a thrust sheet correlated with the Kalak Nappe Complex) shows these typically Baltican detrital populations are of special interest here.

An apparent anomaly in our data is seen in the subsidiary peaks ranging from c. 1.45 to c. 1.0 Ga in formations north of the TKFZ, in the dextrally translated, allochthonous basinal domain. Such Mesoproterozoic ages have hitherto not been reported from the exposed basement of this northern part of the Fennoscandian Shield, and could be attributed to Laurentian sources. However, it is perfectly conceivable that rock complexes of Mesoproterozoic age (associated with Grenvillian magmatism) may be present in the ***concealed*** Baltican basement, i.e., beneath the Caledonian nappes and parts of the continental shelf, and thus provided some of the detritus in the fluvial to deltaic formations now forming the allochthon northeast of the TKFZ. An alternative interpretation would be that parts of the hidden pericraton beneath the nappes may belong to an exotic microcontinental block welded onto Baltica prior to the inception of Neoproterozoic basinal sedimentation.